DOE/NASA/0235-1
NASA CR-165597
UTRC-915395-12

Extension to an Analysis of Turbulent Swirling Compressible Flow for Application to Axisymmetric Small Gas Turbine Ducts

O.L. Anderson
G.B. Hankins
D.E. Edwards
United Technologies Research Center

February 1982

Prepared for
NATIONAL AERONAUTICS AND SPACE ADMINISTRATION
Lewis Research Center
Under Contract DEN 3-235

for
U.S. DEPARTMENT OF ENERGY
Conservation and Solar Energy
Office of Transportation Programs

DOE/NASA/0235-1
NASA CR-165597
UTRC-915395-12

Extension to an Analysis of Turbulent Swirling Compressible Flow for Application to Axisymmetric Small Gas Turbine Ducts

O.L. Anderson
G.B. Hankins
D.E. Edwards
United Technologies Research Center

February 1982

Prepared for
National Aeronautics and Space Administration
Lewis Research Center
Cleveland, Ohio 44135
Under Contract DEN 3-235

for
U.S. DEPARTMENT OF ENERGY
Conservation and Solar Energy
Office of Transportation Programs
Washington, D.C. 20545
Under Interagency Agreement DE-AI01-77CS51040

1. Report No.	2. Government Accession No.	3. Recipient's Catalog No.
NASA CR-165597		

4. Title and Subtitle	5. Report Date
Extension to an Analysis of Turbulent Swirling Compressible Flow for Application to Axisymmetric Small Gas Turbine Ducts	December 1981
	6. Performing Organization Code
7. Author(s)	8. Performing Organization Report No.
O. L. Anderson, G. B. Hankins, Jr., D. E. Edwards	R81-915395-12
	10. Work Unit No.
9. Performing Organization Name and Address	
United Technologies Research Center East Hartford, CT 06108	11. Contract or Grant No. DEN3-235
	13. Type of Report and Period Covered Contract Report Nov. 1980-Nov. 1981
12. Sponsoring Agency Name and Address	14. Sponsoring Agency Code /Rpt. No.
National Aeronautics and Space Administration, Lewis Research Center, 21000 Brookpark Road Cleveland, OH 44135	DOE/NASA/0235-1

15. Supplementary Notes

NASA Project Manager: K. L. McLallin
UTRC Project Manager: O. L. Anderson
Final report prepared under Interagency Agreement No. DEAI 01-77CS51040

16. Abstract

An existing computer program, the Axisymmetric Diffuser Duct Code (ADD code), which calculates compressible turbulent swirling flow through axisymmetric ducts has been modified to permit calculation of flows through small gas turbine ducts with struts, guide vanes and large degrees of turning. The code improvements include a new coordinate generator, an end-wall loss model, and a generalized geometry capability to describe struts and guide vanes in ducts which turn more than 90 degrees. An improved output format has been developed to provide the solution on any arbitrary plane in the duct and an extensive literature survey of calculation procedures used in gas turbine technology has been completed which suggests future improvements in the computer code. Calculations are presented for the flow through the AGT101 small gas turbine inlet duct and turbine exhaust diffuser which demonstrate the ADD code modifications implemented in the present investigation. The computed results compare favorably with experimental results.

17. Key Words (Suggested by Author(s))	18. Distribution Statement
Turbulent, Swirling, Compressible, Axisymmetric, Gas Turbine Flow.	Unclassified, Unlimited Star Category 85 DOE Category UC-96

19. Security Classif. (of this report)	20. Security Classif. (of this page)	21. No. of Pages	22. Price*
Unclassified	Unclassified	67	

* For sale by the National Technical Information Service, Springfield, Virginia 22151

Extension to an Analysis of Turbulent Swirling Compressible Flow For Application to Axisymmetric Small Gas Turbine Ducts

TABLE OF CONTENTS

		Page
1.0	SUMMARY	1
2.0	INTRODUCTION	2
3.0	ANALYSIS	5
	3.1 Coordinate Generator	5
	3.2 Endwall Loss Calculation	12
	3.3 Blade Geometry Calculation	15
	3.4 Interpolation to Arbitrary Line	17
	3.5 Literature Survey of Gas Turbine Calculations	19
4.0	RESULTS	24
	4.1 Comparison of Coordinate Generators	24
	4.2 AGT101 Turbine Inlet Duct	26
	4.3 AGT101 Turbine Exhaust Diffuser	28
5.0	CONCLUSIONS AND RECOMMENDATIONS	30
6.0	REFERENCES	31
7.0	LIST OF SYMBOLS	36
8.0	FIGURES	39

1.0 SUMMARY

An existing computer program, the Axisymmetric Diffuser Duct Code (ADD code), which calculates compressible turbulent swirling flow through axisymmetric ducts has been modified to permit calculation of flows through small gas turbine ducts with struts, guide vanes and large degrees of turning. The code improvements include a new coordinate generator, an end-wall loss model, and a generalized geometry capability to describe struts and guide vanes in ducts which turn more than 90 degrees. An improved output format has been developed to provide the solution on any arbitrary plane in the duct and an extensive literature survey of calculation procedures used in gas turbine technology has been completed which suggests future improvements in the computer code. Calculations are presented for the flow through the AGT101 small gas turbine inlet duct and turbine exhaust diffuser which demonstrate the ADD code modifications implemented in the present investigation. The computed results compare favorably with experimental results.

2.0 INTRODUCTION

The NASA-Lewis Research Center and the Department of Energy is conducting a program to develop turbine technology for automotive gas turbine application. Development of the AGT101 Engine in the Automotive Gas Turbine Engine Program requires not only a component test program, but also the development of accurate and reliable analyses to support the program. Thus, a computer analysis for predicting the turbulent swirling compressible flow in axisymmetric ducts with struts and guide vanes for application to the design of small gas turbine engines would support this program and would be suitable for more general use in small engine design and development.

The Axisymmetric Diffuser Duct analysis (ADD code) developed by Anderson (Refs. 1 and 2) has been shown to produce accurate and reliable calculations of flows in gas turbine engine components. It has been successfully applied to predicting the performance of the subsonic portion of mixed compression inlets (Bowditch Ref. 3) and to predicting the pressure recovery of high Mach number diffusers (Povinelli Ref. 4). Additional applications have been to straight wall annular diffusers, effects of inlet distortion on diffuser performance, and mixing to two coaxial streams, (Anderson Ref. 5) and further calculations were made for swirling flow in a precombustion diffuser and for an inlet with inlet guide vanes (Barber, et al., Ref. 6). Finally, the ADD code has been applied to the solution of flows in small axial flow turbines (McLallin and Kofskey Ref. 7) and recently, it has been modified to treat flows with a small separation bubble, flows with large compressible axisymmetric streamline curvatures, and nonequilibrium turbulent flows which require a two equation (k, ε) turbulence model (Anderson and Edwards Ref. 8).

The ADD code, with some modifications, can be applied to the solution of flows in annular ducts which have significant radial flow components as found in small gas turbine engines. Although the basic solution algorithm used to solve the viscous flow has no restrictions as to flow turning, the algorithm used to calculate the coordinate mesh is limited to ducts which make less than a 90 deg turn. A new algorithm, developed by Davis (Ref. 9), has no such restriction. In addition, the Davis method employs a second order integration formula which exactly integrates the singularities (poles) which occur at each corner of the n-sided polygon used to represent the duct with a Schwartz-Christoffel transformation. This method is used to generate a coordinate mesh which is constructed from the streamlines and potential lines of the plane potential flow solution obtained from the Schwartz-Christoffel transformation. Because of the exact treatment of the poles, this new algorithm can be expected to be more accurate (Sridhar and Davis Ref. 10). Therefore, the first part of the analysis section deals with the incorporation of the Davis algorithm into the ADD code. Comparisons are made with the original coordinate generator and cases are calculated for the flow through two ducts typical of small gas turbine engines and results are compared with experimental data.

In the present approach strut and guide vane effects appear in the governing turbulent flow equations as gap-averaged a-priori body forces. These body forces are obtained using blade element theory which treats the mainstream flow through the cascade as if it were two dimensional and inviscid (see Johnson and Bullock, Ref. 11, and Barber, et al., Ref. 6). The airfoil section cascade performance is obtained using empirical data. The present version of the ADD code contains these empirical relations for NACA 65 series airfoils and NACA four digit series airfoils (Abbott Ref. 12). This procedure using the ADD code, has been shown by Barber, et al. (Ref. 6) to produce good predictions of the flow field through a compressor inlet guide vane. In particular, the exit flow angles, the mean streamwise velocities, and the mean cross flow velocities in the endwall boundary layer were shown to be modeled quite well. The loss mechanism, however, only accounted for blade profile loss and end-wall friction loss. A number of authors, Hanley (Ref. 13), Papailiou, et al. (Ref. 14) and Koch and Smith (Ref. 15) have developed endwall loss models to account for three dimensional effects in the blade passage. The second part of the analysis section describes a simple model, based on the Papailiou correlation, which has been incorporated into the code.

The initial version of the ADD code had limited applicability to small gas turbine ducts with struts and guide vanes because the code used cylindrical (r, x, ϕ) coordinates to describe the strut geometry. In this, the blade centerline was located using the axial distance as an independent variable and the blade chord, thickness, and camber were described using the radial distance r as the stacking line (independent variable). Clearly, this procedure is inadequate to treat small gas turbine ducts which may turn more than 90 deg because data may be multivalued along either r or z. The third part of the analysis section deals with a new approach to describe the duct and blade geometry. This new generalized analysis will be demonstrated by calculating the flow through two ducts, typical of small radial gas turbine engines, which have supporting struts or guide vanes.

The fourth part of the analysis section deals with a modified output format. In the initial version of the code the solution, which is calculated in the (s,n) coordinate system where s is along inviscid streamlines and n along potential lines, is printed along coordinate lines (s = const). Experimental data is seldom available along these coordinate lines so that comparison with calculated results is difficult. The fourth part of the analysis deals with the interpolation and resolution of the vector and tensor quantities along any arbitrary experimental data line.

Small gas turbine ducts with struts and guide vanes generate three dimensional flows which in gas turbine technology are called secondary flows. In addition, rotors and stators generate tip leakage effects due to the large pressure difference across the blades. These secondary flows produce two principal effects on the gap average flows as pointed out by Square and Winter (Ref. 16). The first effect is called "overturning" and occurs in the endwall boundary layer region where the flow turns more than would be predicted by a simple two dimensional analysis or data

correlations. The second effect is called "corner loss" and is produced by the corner flow in the form of a vortex roll up and/or corner stall. At the present time the ADD code does not model these important three dimensional effects although it has demonstrated that some important features of the flow through ducts with struts and guide vanes such as "overturning" are modeled (see Barber, et al. Ref. 6). A large body of literature exists which attempts to model these effects in axial flow compressors using gap averaged equations similar to the equations used in the ADD code. Therefore, the last part of the analysis deals with a literature survey of attempts to model these endwall secondary flow effects as they occur in turbomachinery with a view toward incorporating or developing a model for use in the ADD code in the future.

3.0 ANALYSIS

3.1 Coordinate Generator

An ideal coordinate system should facilitate the formulation and numerical solution of the viscous flow solver. It should ease the expression of boundary conditions and minimize the truncation error due to difference approximations of the flow equations. In addition, the analysis on which the ADD code is based required that the coordinate system be orthogonal and that it be a first approximation to the viscous flow through the duct since the flow curvature is assumed to be the same as that of the streamwise coordinate lines (see Anderson (Ref. 1)). A two dimensional orthogonal coordinate system, suitable for the ADD code, can always be constructed from a potential flow solution by setting the normal coordinate equal to the stream function and the streamwise coordinate equal to the velocity potential. For plane flow, conformal mapping techniques are ideal because it allows solution of the inverse problem by direct means. That is (x(s,n), y(s,n)) rather than (s(x,y), n(x,y)) can be calculated directly where (x,y) is the Cartesian system and (s,n) curvilinear system. For many ducts, this plane flow solution serves as a sufficiently good approximation to the flow curvature of axisymmetric flow. However, for certain cases where this approximation is insufficient, a technique has been developed by Anderson and Edwards (Ref. 8) to obtain axisymmetric streamline curvatures for use with the coordinate system derived from plane potential flow. Thus, coordinate grids based on conformal mapping appear ideal for use in the ADD code.

Of the many mapping functions possible, one based on the Schwartz-Christoffel transformation is ideal because it can be applied to any arbitrary duct likely to be encountered in fluid flow problems. Anderson (Ref. 1) and Davis (Ref. 9) have developed mapping techniques based on the Schwartz-Christoffel transformation, for constructing coordinate grids. Anderson's method, which uses polygonal (straight) elements to represent the duct contour avoids the problem posed by the poles (singularities) by integrating along a path just inside the wall boundary. Davis extended the mapping procedure to include both straight lines and curved line elements. Another feature of the Davis procedure is the use of a composite finite difference formula which integrates exactly the poles at each corner point and thus treats the duct geometry exactly. The Davis method has been applied to internal flow duct problems by Sridhar and Davis (Ref. 10) in which it was shown that the method produces second order accurate coordinates and metric coefficients. This procedure has been selected and adapted in the present investigation to replace the original ADD code coordinate generator.

Schwartz-Christoffel Transformation

A two step transformation, shown on Fig. 1, is adopted. This first step is the Schwartz-Christoffel transformation from the duct (z) plane to the upper half (ζ) plane.

$$\frac{dz}{d\zeta} = M \prod_{i=1}^{N} (\zeta - b_i)^{-\alpha_i/\pi} \qquad (3.1.1)$$

This mapping has a constant M which determines the rotation of the duct relative to the real axis. The corner angles are denoted by α_i and are known. The pole locations b_i in the ζ plane, however, are not known.

The second step of the transformation is from the upper half (ζ) plane to a straight channel in the t plane

$$t = -\frac{1}{\pi} \ln \zeta + i \qquad (3.1.2)$$

If t is the complex potential

$$t = s + in \qquad (3.1.3)$$

where s is the velocity potential and n is the stream function, then construction of a cartesian mesh in the t plane represents a conformal mesh in the z plane composed of the stream function and velocity potential for the plane potential flow through the duct. The complex conjugate of the potential flow velocity is

$$u - iv = \frac{dt}{dz} \qquad (3.1.4)$$

Hence, the magnitude of the potential flow velocity is

$$V = \left| \frac{dt}{dz} \right| \qquad (3.1.5)$$

which is the inverse of the metric coefficient.

The mapping shown in Fig. 1 places certain restrictions on the use of the ADD code algorithm which should be understood at this time. It is noted on Fig. 1 that the polygon representing the duct is closed at infinity. Thus, the duct is extended to infinity along the dotted straight lines as shown. It is assumed, in this mapping, that the duct inlet is a straight channel with parallel walls, but the duct exit may be a divergent channel with a divergence angle α_e which must be greater than zero. If one considers the duct alone, this potential flow solution is not the

only solution since one is free to impose any boundary condition of the proper type along the inlet boundary (z_1 to z_N) and exit boundary (z_{NLF} to Z_{NLF+1}). Therefore, the mapping predetermines the streamline curvature at the inlet and exit of the duct.

Equation (3.3.1) can be reduced to a form involving only poles and angles on the duct. This form is given by

$$\frac{dz}{d\zeta} = \frac{M}{\zeta}\,\zeta^{-\alpha_e/\pi} \prod_{i=1}^{N} (\zeta - b_i)^{-\alpha_i/\pi} \tag{3.1.6}$$

Integration of the Transformation

The transformation given by Eq. (3.1.6) is singular at each pole b_i. Davis (Ref. 9) has developed a composite finite difference formula by analytically integrating Eq. (3.1.6) in the neighborhood of the poles. This formula is given by

$$z_{K+1} = z_K + \frac{M}{\zeta_{K+1/2}}\,\zeta_{K+1/2}^{-\frac{\alpha_e}{\pi}} \prod_{i=1}^{N} \left\{ \frac{(\zeta_{K+1}-b_i)^{-\frac{\alpha_i}{\pi}+1} - (\zeta_K - b_i)^{-\frac{\alpha_i}{\pi}+1}}{(\zeta_{K+1}-\zeta_K)\left(-\frac{\alpha_i}{\pi}+1\right)} \right\} (\zeta_{K+1}-\zeta_K) \tag{3.1.7}$$

From Eq. (3.1.2) we have

$$\zeta_{K+1} - \zeta_K = -\pi\,\zeta_{K+1/2}\,(t_{K+1} - t_K) \tag{3.1.8}$$

which may be combined with Eq. (3.1.7) to provide a direct integration to the t plane. These equations, as demonstrated by Sridhar and Davis (Ref. 10), are second order accurate and contain no singularities. Therefore, the integration may be done along the walls which contain the poles. Equations (3.1.7) and (3.1.8) may be used to integrate along either streamlines or potential lines. Thus, we have

$$dt = ds + i\,dn \tag{3.1.9}$$

By setting dn = 0 the integration is along streamlines and by setting ds = 0 the integration is along potential lines.

Asymptotic Solution

The asymptotic solution for far upstream in the straight inlet channel is obtained as $\zeta \to \infty$. Equation (3.1.1) reduces to

$$\frac{dz}{d\zeta} = \frac{M}{\zeta} \tag{3.1.10}$$

Integrating Eq. (3.1.10) and substituting Eq. (3.1.2), we have

$$z = \pi M(i-t) + z_0 \tag{3.1.11}$$

Subtracting the lower wall from the upper wall results in

$$z_U - z_L = -\pi M_i \tag{3.1.12}$$

The height of the duct (see Fig. 2) is given by

$$H = \left| z_U - z_L \right| \tag{3.1.13}$$

Hence, Eq. (3.1.12) becomes

$$z_U - z_L = He^{i(\theta + \pi/2)} \tag{3.1.14}$$

where θ is the angle between the duct and the real axis. Solving for M we have

$$M = -\frac{H}{\pi} e^{i\theta} \tag{3.1.15}$$

Thus, M scales the height and rotation of the duct.

Iteration Procedure

An examination of Eqs. (3.1.6) and (3.1.2), together with Fig. 3 shows that the α_i's and line segments $|z_{ci+1} - z_{ci}|$ are known along the walls but the location of the poles b_i or t_i are not known. One constant can be fixed arbitrarily so that we take (z_1, b_1, t_1) as known. For the moment, let us assume (z_N, b_N, t_N) are known. Then new guesses for the poles b_i's are given by comparing the lengths of line segments

$$t_i^{\nu+1} = t_{i-1}^{\nu+1} + \frac{\left|z_{ci} - z_{ci-1}\right|}{\left|z_i^{\nu} - z_{i-1}^{\nu}\right|}\left(t_i^{\nu} - t_{i-1}^{\nu}\right) \tag{3.1.16}$$

and from Eq. (3.1.2)

$$b_i^{\nu+1} = \exp\left[\pi\left(i - t_i^{\nu+1}\right)\right] \tag{3.1.17}$$

Absolute and uniform convergence is established when all points satisfy the condition

$$\left|z_{ci} - z_i^{\nu}\right| < \epsilon \tag{3.1.18}$$

The iteration formula given by Eq. (3.1.16) is valid for all points except $t_N^{\nu+1}$. This point is determined using the asymptotic solution in the following manner. Let us define for upstream t_1' and t_N', shown in Fig. 4, by the following relations

$$\left.\begin{aligned} t_1' &= t_1 - \sigma\left|t_1\right| \\ t_N' &= t_1' + i \end{aligned}\right\} \tag{3.1.19}$$

where σ is a parameter chosen to move t_1' sufficiently far upstream to approximate the limiting asymptotic solution as $t \to -\infty$. Referring to Fig. 4, the point z_N^{ν} is determined with known t_i^{ν}'s by integrating along the path (z_{c1} to A to z_N^{ν}). Then the point z_1' is determined by integrating along the path (z_1 to z_1'). The point z_N' is determined using the asymptotic solution (Eq. 3.1.12). Hence,

$$z_N' - z_1' = -\pi M i \tag{3.1.20}$$

Then the point $t_N^{\nu+1}$ is given by

$$t_N^{\nu+1} = t_N' + \frac{\left|z_{CN} - z_N'\right|}{\left|z_N^{\nu} - z_N'\right|}\left(t_N^{\nu} - t_N'\right) \tag{3.1.21}$$

A closure error may be defined by integrating along the two paths from (z_{c1} to z_{NLF+1}). Then,

$$\epsilon_c = \left|(z_{NLF+1})_{path\,1} - (z_{NLF+1})_{path\,2}\right| \tag{3.1.22}$$

Approximate Potential Flow Solution

The iteration algorithm described above converged for most ducts with arbitrary initial guesses for the poles b_i. The rate of convergence (number of iterations), however, was found to depend strongly on the complexity of the duct and as expected more complex shapes were found to converge more slowly. For the AGT 101 duct described in the next section, convergence could not be obtained with arbitrary guesses for b_1. Hence, it was decided to obtain an initial guess for b_i from an approximate potential flow solution which could be obtained by geometric construction.

The method of geometric construction is shown on Fig. 5. This consists of constructing a mean line z_m and normals to the mean line which approximate potential lines. The three unknown points, $z_{UI,J}$, $z_{m,J}$, $z_{LI,J}$, shown on Fig. 5, must satisfy the following relations

$$\left|z_{m,J} - z_{m,J-1}\right| = \Delta x_s \tag{3.1.23}$$

$$1 - \frac{\left|z_{UI,J} - z_{m,J}\right|}{\left|z_{m,J} - z_{LI,J}\right|} = D \tag{3.1.24}$$

$$(z_{UI,J} - z_{LI,J}) \cdot (z_{m,J} - z_{m,J-1}) = 0 \tag{3.1.25}$$

The parameter Δx_s is any arbitrary length and the parameter D is nominally zero to determine the midpoint. Equation (3.1.25) sets orthogonality for the mean line and potential line. Since the duct wall is composed of straight line segments with discontinuous slope, D cannot always be zero. Therefore, it was decided to set up an iteration procedure to find a slope which would minimize D.

The solution to Eq. (3.1.23) through Eq. (3.1.25) is as follows. Let us define an angle θ_J^ν such that

$$z_{m,J}^\nu = z_{m,J-1} + \Delta x_s \left[\cos\theta_J^\nu + i \sin\theta_J^\nu\right] \tag{3.1.26}$$

A straight line normal to the mean line is defined by the points $z^{\nu}_{m,J}$ and the point

$$\tilde{z} = z_{m,J} + \Delta x_s\left[\cos(\theta^{\nu}_J + \frac{\pi}{2}) + i\sin(\theta^{\nu}_J + \frac{\pi}{2})\right] \tag{3.1.27}$$

A search of the input wall data is made for the intersections $z^{\nu}_{UI,J}$ and $z^{\nu}_{LI,J}$. The parameter D is calculated from Eq. (3.1.24). Then, successive guesses are made for θ^{ν}_J to minimize D.

The potential flow velocities are calculated by assuming that the velocity on the mean line satisfies the continuity equation and the velocities on the wall satisfy the angular momentum equation locally. Hence, we have the following relations

$$H_J = \left| z_{UI,J} - z_{LI,J} \right| \tag{3.1.28}$$

$$K_{m,J} = \left(\frac{d\theta}{dx_s}\right)_J \tag{3.1.29}$$

$$V_{m,J} = 1/H_J \tag{3.1.30}$$

where $K_{m,j}$ is the curvature and $V_{m,j}$ is the velocity on the mean line.

Then define a function ϕ given by

$$\phi = \frac{1 - K_{m,J}/(2V_{m,J})}{1 - K_{m,J}/(2V_{m,J})} \tag{3.1.31}$$

and the wall velocities are given by

$$V_{UI,J} = \frac{2}{1+\phi}\ V_{m,J} \tag{3.1.32}$$

$$V_{UL,J} = \frac{2\phi}{1+\phi} V_{m,J} \tag{3.1.33}$$

These approximate velocities can be used to integrate Eq. (3.1.5) to obtain the approximate t_i locations for each z_i corner in the Z plane. The initial guess for the b_i's is then obtained from Eq. (3.1.17).

3.2 Endwall Loss Calculation

Struts and guide vanes are treated as a-priori body forces applied to the turbulent flow equations as described by Barber, et al. (Ref. 6). Empirical cascade data (turning angle and loss) or empirical airfoil data (lift and drag) are used to calculate the two dimensional blade section forces. The interaction of the blade boundary layer with the endwall boundary layer can be treated by adding an endwall loss to the profile loss in the calculation procedure.

The endwall loss coefficient can be defined with respect to the upstream inviscid flow by

$$Z_{EW} = (P_{T1} - P_{T2})/(\tfrac{1}{2}\,\tilde{\rho}_1\,\tilde{U}_1^2) \tag{3.2.1}$$

where P_{T1} and P_{T2} are the gap averaged viscous total pressures upstream and downstream of the blade row and $(1/2\ \tilde{\rho}_1\ \tilde{U}_1^2)$ is the inviscid gap averaged dynamic pressure upstream of the blade row. It is further assumed that the flow is incompressible and that the endwall boundary layers are thin so that the inviscid velocity is the velocity at the edge of the boundary layer. Under these conditions, Eq. (3.2.1) can be written as

$$Z_{EW} = \left(\frac{\tilde{U}_{2e}}{\tilde{U}_{1e}}\right)^2 \left[1 - \left(\frac{U_2}{U_{2e}}\right)^2\right] - \left[1 - \left(\frac{U_1}{U_{1e}}\right)^2\right] \tag{3.2.2}$$

We note from Eq. (3.2.2) that at the edge of the endwall boundary $z_{Ew} = 0$ and at the wall $Z_{Ew} = (\tilde{U}_{2e}/\tilde{U}_{1e})^2 - 1$.

Hanley (Ref. 13) developed a correlation for the gap averaged boundary layer profiles in a cascade based on Coles (Ref. 17) two dimensional boundary layer profiles. However, these correlations are difficult to use. Mager, et al. (Ref. 18) has shown that if the cross flow component is neglected, a one parameter family of power law profiles can be used to represent the velocity profiles. This one parameter family of profiles can be integrated over the boundary thickness to establish the relations between displacement thickness, momentum thickness and shape factor, in terms of the descriptive parameter. Hence, if the shape factor and momentum thickness are known, then the loss can be determined from the family of velocity profiles. Papailiou, et al. (Ref. 14) has developed a correlation relating the upstream and downstream momentum thickness to a pressure rise parameter across the cascade. This procedure will be used here. Let

$$\frac{U}{U_e} = \left(\frac{y}{\delta}\right)^{1/n} \qquad y \le \delta \tag{3.2.3}$$

$$\frac{U}{U_e} = 1 \qquad y > \delta \tag{3.2.4}$$

where the shape factor H and displacement thickness δ^* are given by

$$H=(2+n)/n \tag{3.2.5}$$

$$\delta/\delta^{*} = 1+n \tag{3.2.6}$$

The correlation given by Papailiou is

$$\frac{\theta_2}{\theta_1} = \left(\frac{U_1}{U_2}\right)^3 (1+B)^{5/6}/AVR \tag{3.2.7}$$

$$B = \left(\frac{c_f}{2\theta_1/C}\right)^{6/5} \frac{\left(\frac{U_1}{U_2}\right)^{4.4}}{4.4\left(\frac{U_1}{U_2}\right)^{3.4}\left[\left(\frac{U_1}{U_2}\right)-1\right]} \tag{3.2.8}$$

$$AVR = U_{s2}/U_{s1} \tag{3.2.9}$$

An estimate of the friction coefficient can be obtained from the Ludweig-Tillman law (Ref. 19)

$$C_f = 0.246 \times 10^{-.678H} Re_\theta^{-.268} \tag{3.2.10}$$

where

$$Re_\theta = \rho_1 U_1 \theta_1/\mu_1 \tag{3.2.11}$$

The shape factors, based on experience of other authors (see literature survey) is taken to be 1.6 and 2.0, respectively. These shape factors may be considered empirical constants which may be used to fit the predictions of loss with experimental data.

At the present time experimental data does not exist to evaluate the endwall loss model as applied to struts and guide vanes in small radial gas turbine engines. Therefore, a representative case was calculated to demonstrate the effect of adding the endwall loss to the profile loss and the results are shown in Fig. 6. This representative case is for an exit guide vane in a gas turbine exhaust nozzle which is described in Section 4.1. It is clearly shown in Fig. 6 that the endwall loss model significantly adds to the total loss of the blade.

3.3 Blade Geometry Calculation

A stacking plane passing through the axis of symmetry (z axis) is defined as shown in Fig. 7. The x and y axis are then defined in the (r,z) plane by the location of the origin (r_{CLO}, z_{CLO}) and rotation with respect to the axis of symmetry θ_{CL}. In this coordination system, the y axis is defined as the stacking line (independent variable) and all blade characteristics are defined as functions of y. These blade characteristics are the blade centerline location x_{CL} (y), blade chord c(y), stagger angle α_s(y), thickness to chord ratio t/c(y), and equivalent circular arc camber angle ϕ_c(y). The stagger angle is the angle between the blade chord line and the axis of symmetry. Hence, the projection of the blade chord on to the (r,z) plane or stacking (x,y) plane is given by

$$x_c = c \cos \alpha_s \tag{3.3.1}$$

The projection of the chord line is shown in both Figs. 7a and 7b.

The transformation of a point in the stacking (x,y) plane to a point in the (r,z) plane is given by

$$r = r_{CLO} + x \sin \theta_{CL} + y \cos \theta_{SL} \tag{3.3.2}$$

$$z = z_{CLO} + x \cos \theta_{CL} - y \sin \theta_{CL} \tag{3.3.3}$$

This transformation may then be applied to the blade centerline coordinates x_{CL}(y) to calculate r_{CL}(y) and z_{CL}(y) in cylindrical coordinates for all of the input data points defining the blade characteristics. These centerline points must be located in the ADD code (n,s) coordinate system. A search is then made of the coordinate file (r(n,s), z(n,s)) for, as an example, the Lth blade data point, to determine the coordinate grid containing the point as shown on Fig. 8a. With S_j, S_{j+1}, n_k, n_{k+1} known, a bivariate interpolation is used to determine the coordinate point (n_L, s_L). In this manner a table x_{CL}(y), c(y), α_s(y), t/c(y), ϕ_c(y), r_{CL}(y), z_{CL}(y), x_{SCL}(y), n(y), s(y) is constructed which completely describes the blade.

As the viscous flow calculation proceeds, the point n_k, s_j is known and the problem becomes one of finding the corresponding point in the stacking plane so that the blade properties are known. This procedure is shown on Fig. 8b. The n_k streamline crosses the blade centerline between the n_L, n_{L+1} points on the table. A univariate interpolation is then used to obtain all blade characteristics for the n_kth streamline. The blade leading edge in the (r,z) plane is located by the arc length distance along the n_kth streamline.

$$x_{SLE} = x_{SCL} - x_C/2 \tag{3.3.4}$$

Therefore, the point s_J, n_k is located at

$$\frac{x}{C} = \left[x_s(S_J, n_K) - x_{SLE}(n_K)\right] / x_C(n_K)\right] \tag{3.3.5}$$

on the blade chord line and the local blade thickness and other parameters can be determined.

3.4 Interpolation to Arbitrary Line

Let us define an output data line by the coordinate y and its normal x which lie in a plane passing through the axis of symmetry (z axis). Here the normal to the (x,y) plane is in the ϕ direction, and Fig. 8a may be used as an illustration. The solution of the flow field at points distributed along y is required. Clearly, the same transformation and search procedures described in Section 3.3 can be used to produce a table of $r(y_L)$, $z(y_L)$, $n(y_L)$, $s(y_L)$. To simplify the search in the solution data, $J(y_L)$ and $K(y_L)$ are included in the table where (J,K) is one corner point of the grid surrounding the point y_L as shown in Fig. 8a. With J, K known, the flow field variables can be obtained using a bivariate interpolation on (n,s).

There remains the resolution of vector quantities (velocity) and tensor quantities (stresses). Let us define the unit vector in the (s,n,ϕ) ADD code coordinate system by

$$\vec{k}_\ell = (\vec{k}_s \; \vec{k}_n \; \vec{k}_\phi) \tag{3.4.1}$$

and the unit vector in the (x,y,ϕ) by

$$\vec{i}_m = (\vec{i}_x \; \vec{i}_y \; \vec{i}_\phi) \tag{3.4.2}$$

The rotation of vectors involves only one angle, θ, so that the direction cosines are given by

$$\bar{\bar{\alpha}} = \begin{vmatrix} \cos\theta & -\sin\theta & 0 \\ \sin\theta & \cos\theta & 0 \\ 0 & 0 & 1 \end{vmatrix} \tag{3.4.3}$$

Then, if v is the velocity vector in the (x,y,ϕ) system and u the velocity in the (s,n,ϕ) system,

$$v_\ell = \alpha_{\ell m} u_m \tag{3.4.4}$$

Similarly, if $\bar{\bar{\tau}}$ is the stress in the (x,y,ϕ) system and $\bar{\bar{\sigma}}$ the stress in the (s,n,ϕ), then

$$\tau_{ij} = \alpha_{im} \alpha_{\ell j} \sigma_{\ell m} \tag{3.4.5}$$

We should note that assumptions implicit in the ADD code equations are

$$\begin{aligned} \sigma_{nn} &= \sigma_{ss} = \sigma_{\phi\phi} = 0 \\ \sigma_{ns} &= \sigma_{sn} \\ \sigma_{n\phi} &= \sigma_{\phi n} \\ \sigma_{s\phi} &= \sigma_{\phi s} = 0 \end{aligned} \tag{3.4.6}$$

Where σ_{ns} and $\sigma_{n\phi}$ are calculated. If x is aligned with the z axis then (x,y,ϕ) becomes the cylindrical (z,r,ϕ) coordinate system.

3.5 Literature Survey of Gas Turbine Calculations

It is well known that flows in turbomachinery are unsteady, three dimensional, turbulent, compressible and occur in flow passages that are geometrically complex. Since the overall problem of predicting the flow in turbomachinery is so complicated, analysis attempts to solve a much simpler problem in which the neglected complexity is resolved with the use of empirical factors chosen to make predictions agree with experiment. The assumptions used to simplify this problem form the framework of this literature survey which is presented with the point of view of extending the ADD code analysis to treat the more complex flows found in turbomachinery. These assumptions are:

1. Quasi-steady flow assumption
2. Quasi-two dimensional flow assumption
3. Generalized boundary layer assumption
4. End-wall blade force assumption
5. Inviscid secondary flow assumption
6. Turbulent mixing length assumption

The quasi-steady flow assumption states that the flow may be considered steady in time when examined in a coordinate system rotating with the angular velocity of the blade. The work done by a compressor or turbine, when examined in a stationary coordinate system, is done by the time varying pressure field. When the appropriate transformation based on the quasi steady flow assumption is used, the time varying pressure field is converted to a spatially varying pressure field and the Euler equations for turbomachinery are derived. This assumption accounts for the work done by the compressor or turbine but does not account for unsteady effects such as a compressor surge. However, unsteady flow even when considered in the quasi-steady frame of reference still has significant effects, as shown by Dring et al. (Ref. 20), which may have to be taken into account by empirical means. The ADD code analysis and nearly all other analyses use the quasi-steady flow assumption to simplify the analysis.

The quasi two dimensional flow assumption is used to reduce the geometric complexity of the gas turbine passage. It states that the three dimensional flow in the turbomachines can be built up by considering two dimensional flow in three weakly interacting planes. Although three dimensional flow field calculations of the type pioneered by Wu (Ref. 21) are currently under development, these are generally inviscid and hence neglect phenomena which a designer is most interested such as compressor loss and efficiency. The three surfaces may be called the meridional plane surface, the cascade plane surface, and the secondary flow or Trefftz plane surface. The meridional plane surfaces are of two types: 1) a curved surface midway between adjacent blades (S1 surface of Wu), or 2) a meridional plane surface (r, z plane) obtained by circumferentially averaging the flow equations. Almost all current design methods use the second type of surface. Inviscid flow

field solutions in the meridional plane are generally of the matrix through flow type of analysis initiated by Marsh (Ref. 22) and Wu (Ref. 23) or of the streamline curvature type developed by Mellor (Ref. 24), Smith (Ref. 25), and Novak (Ref. 26). Gap averaging of the flow equations to obtain the flow in the meridional plane reduces the spatially varying pressure field to a-priori body forces which are treated by empirical means. The inviscid streamline analysis, such as those described above, incorporate the effects of endwall boundary layer growth using empirical blockage factors. The ADD code uses the meridional plane approach with body forces computed a-priori to represent the blades. However, since it is a viscous solution, endwall blockage is treated directly by solution of the boundary layer flow rather than treated indirectly by empirical factors.

The body forces are determined by examining the flow in the cascade plane which is obtained by unrolling a cylindrical surface passing through the compressor or turbine. The flow in this plane generates the spatially varying pressure field in quasi-steady flow and thus produces work. A large body of literature exists on the analysis of cascade flow or the empirical representation of cascade flow. (See as an example Johnson and Bullock, Ref. 11). The ADD code uses empirical cascade correlations coupled with an inviscid flow analysis, which with known streamline curvature, reduces to the method of Novak (Ref. 26) to calculate the body force for use in the meridional plane calculation. Although the cascade plane concept is useful for analyzing flows in axial flow turbomachinery where the radial component of the flow is small, it is not useful for analyzing flows in radial flow turbomachinery where the radial component is large. For these types of flows, three dimensional analysis may be required. However, one simplified analysis, which could be developed within the existing ADD code framework, is the solution of the gap averaged inviscid flow between two meridional plane (S1) surfaces. These S1 surfaces would be the mean surface passing through adjacent blades and a condition of flow tangency would be the additional boundary condition sufficient to establish a solution.

The third surface or Trefftz plane is used to analyze the secondary flow through the gas turbine passage. This plane is approximately normal to the mean flow direction. Thus, the secondary flow velocity components are the gapwise and spanwise components of velocity. Inviscid vorticity transport theories, which shall be discussed later, are used to solve for the flow in the Trefftz plane and have been moderately successful in predicting secondary flow overturning in the end wall region.

The generalized boundary layer assumption is applied to the gap averaged equations of motion in the meridional plane. It states that the viscous forces are small compared to the dynamic forces and blade forces except in a thin region near the end walls and that this region is small compared to the annulus height. With this assumption the flow field can be separated into a core flow and an endwall boundary layer flow. The core flow is inviscid and rotational with blade forces which do work. The end wall boundary layers are viscous flows which determine the effective blockage. The boundary layer equations for the gap averaged

flow have been derived by Railly and Howard (Ref. 27) and Mellor and Wood (Ref. 28). Horlock and Perkins (Ref. 29) present a fairly complete derivation and summary of these approaches to solve the end-wall boundary layer flow. In all cases a momentun integral approach is used to solve the equations. Neglecting for now the problem of representing the blade force and other nonaxisymmetric or three dimensional effects, the momentum integral approach requires a great amount of empirical data correlation to represent the profile shape for both the axial and tangential boundary layer equations as well as a closure equation to get the turbulent wall shear stress. Consequently, a number of ad-hoc assumptions are made to close the problem and many boundary layer theories have been developed which will be discussed in the next paragraph. The ADD code equations for both the streamwise and tangential flow are solved over the whole flow field by numerical methods which need no data correlations for profile shape. Consequently, as shown by Barber, et al. (Ref. 6), remarkably good end-wall boundary layer profiles can be obtained for both the streamwise and crosswise flow through an inlet guide vane flow passage.

The end-wall blade force assumption was stated explicitly by Mellor (Ref. 28) as "the force exerted by the blade in the end-wall region is identical to that obtained if there were no end-walls". In terms of the ADD code formulation, this assumption may be restated as "the force exerted by the blades on the viscous flow is the same as the force exerted by the blades on the inviscid flow". Although clearly an over-simplification, there is some evidence that it is at least approximately true (see Mellor, Ref. 28). The treatment of the blade force terms, together with the general closure problem introduced by the momentum integral approach has resulted in a large number of analytical solutions. Thus, we have a method by Horlock and co-workers (Refs. 29 through 31), Hirsch and co-workers (Refs. 32 through 36), and finally by Papailiou and co-workers (Refs. 37 through 40). Hirsch and co-workers have generally followed along the lines originally suggested by Mellor (Refs. 28, 41, 42) using blade defect forces. Papailiou and also Horlock have followed paths which use the results of secondary flow analysis. Two conclusions may be drawn from a survey of this literature. First, the blade defect forces are important in limiting the growth of the end-wall boundary layer in a multistage compressor. Second, secondary flow effects such as the passage vortex produced by tip leakage limits stage efficiency and work output and should be accounted for.

The major contribution of the blade defect force are additional losses, over and above blade profile loss. This loss is produced by three dimensional corner stall. Empirical correlations for predicting end-wall losses have been developed by Hanley (Ref. 13), Papailiou, et al. (Ref. 14), and Koch (Ref. 15). The correlations developed by Papailiou have been incorporated into the ADD code. Predictions of tip clearance effects using secondary flow theory generally follow along the lines proposed by Lakshminarayana (Ref. 43). These effects are not currently modeled in the ADD code.

Secondary flows which produce spanwise and gapwise velocity components are generally treated using inviscid vorticity transport theory. These theories assume a weak interaction between the primary or through flow and the secondary flow. This assumption is valid if the turning angles are small and/or the vorticity is small. Under these conditions inlet vorticity produced by the end-wall boundary layer is convected along the known primary flow streamlines and is thus known at the exit plane. Secondary vorticity, defined as the component of vorticity in the streamwise direction, is produced by rotation of the inlet vorticity vector. Vorticity produced at the wall boundary and diffusion of vorticity are neglected. The known secondary vorticity distribution at the blade exit plane, together with a continuity relation, is sufficient to solve for the gapwise and spanwise secondary flow in the Trefftz plane. This method was pioneered by Squire and Winter (Ref. 16) and refinements have been developed by Hawthorn (Refs. 44 through 47), by Horlock and Laksminarayana (Refs. 48 and 49) and finally by Smith (Ref. 50). This approach has been quite successful in predicting secondary flow endwall overturning but has been less successful in predicting endwall loss since loss is basically a viscous phenomena.

Although secondary flow losses are generally small, secondary flow mixing can be quite significant. Adkins and Smith (Ref. 51) have developed a secondary flow mixing model which predicts observed flow conditions which cannot be explained in any other manner. This approach treats the secondary flow as a large turbulent eddy on the scale of the blade gap. The spanwise and gapwise velocities produced by this large scale eddy contribute a net exchange of momentum and energy through Reynolds stress type terms which are obtained from the gap averaged equations of motion. Adkins and Smith show that these Reynolds stress type terms can be treated by gradient diffusion terms in which an effective mixing coefficient, in place of an eddy viscosity, is a function of the secondary flow parameters. This analysis of Adkins and Smith can be incorporated into the ADD code since unlike the other theories it covers the whole flow field from wall to wall and could substantially upgrade the ADD code analysis to treat more complex gas turbine flows.

The last assumption is a turbulent mixing length assumption. All of the end-wall boundary layer theories cited above assume that the turbulence in the endwall boundary layer is the same as the turbulence in a two-dimensional boundary layer. Thus, the closure equations developed for two dimensional boundary layers are used. The ADD code makes a similar assumption and uses either an algebraic turbulence model or a two equation turbulence model (Anderson and Edwards, Ref. 8). Although such an assumption may be valid in any given plane, it is not necessarily valid for the gap averaged flow. However, the various solutions of Papailiou, Hirsh, and Horlock cited above appear to give reasonable results for the momentum integral equations and the results of Barber, et al. (Ref. 6) appear also to give a reasonable representation of the turbulence effects.

In summary, it can be seen that the ADD code formulation of the equations of motion which describe the flow through turbomachinery is compatible with the existing literature on the subject. These equations are quasi-steady flow equations for the gap average flow in the meridional (r,z) plane. Body forces are calculated, a-priori, using empirical correlations coupled to an inviscid flow field analysis which reduces to the method of Novak (Ref. 26) when streamline curvature is known. The viscous equations used in the ADD code are essentially identical to the endwall boundary layer equations derived by Mellor (Ref. 28) and Horlock (Ref. 29) and differ only in that they apply to the whole flow field and not to just the endwall region. The turbulence models used in the ADD code and endwall boundary layer analysis of Mellor and Horlock are also equivalent. Since numerical methods are used to solve the equations rather than momentum integral methods, data correlations for profile shape are not required and remarkably good solutions for the endwall boundary layers have been obtained by Barber et al. (Ref. 6). In particular, the endwall overturning can be predicted. A major component of the blade defect force (see Mellor, Ref. 28) is the corner loss. This corner loss is partially accounted by the loss model suggested in Section 3.2 although it has not been verified by comparison with data. Two areas of possible improvement to the ADD code remain. This first is the incorporation of a secondary flow mixing model such as suggested by Adkins and Smith (Ref. 51). The second is the prediction of blade forces in radial flow compressors and turbines.

4.0 RESULTS

4.1 Comparison of Coordinate Generator

The original coordinate generator used in the ADD code was developed by Anderson (Ref. 1). This grid generation method is based on a conformal mapping procedure using the Schwartz-Christoffel transformation. Integration across singular points (poles) at each corner was avoided by choosing a boundary a small distance inside the duct. The integration itself was done using a fourth order Rung-Kutta formula. The method of Davis (Ref. 9), also based on the Schwartz-Christoffel transformation, treats the singular points (poles) using a composite integration formula which is second order accurate and is exact across the poles. Use of this composite integration formula permits integration to take place along the wall boundaries and eliminates the need for the approximation used by Anderson. In addition to improved numerical integration formula, an improved closure procedure was developed by integrating from one wall of the duct to the other wall along a potential line. This new closure procedure permits the construction of coordinates for ducts with arbitrary contours which may turn more than 90 degrees.

A comparison of the two grid generators was made by choosing a simple engine exhaust nozzle, calculating the coordinates using both the Anderson and Davis methods, and then calculating the viscous flow through the nozzle using the ADD code viscous solver. A stretching function suggested by Roberts (Ref. 52) was used to distort the geometric mesh in order to have an adequate distribution of points near the walls for a viscous flow calculation. Each grid generator calculated a geometric mesh consisting of 50 equally spaced streamlines and 80 potential lines as shown in Fig. 9. The new generator obtained uniform and absolute convergence with a tolerance of 10^{-4} in 7 iterations. The computational (CPU) time on a UNIVAC 1100/81A system was 15 1/2 minutes for the new grid generator and 15 minutes for the old generator.

The two grid generators produced essentially identical results for the wall boundaries as can be seen in Figs. 10 and 11 which are comparisons of the inner and outer wall coordinates for the exhaust nozzle calculated by both methods. This was expected since the two methods are based on the Schwartz-Christoffel transformation. However, as can be observed from Figs. 12 and 13, which are comparisons of the metric coefficients along the inner and outer walls using both grid generators, the new generator calculates smoother metric coefficients.

Numerical meshes (Fig. 14) consisting of 80 nonuniformly spaced streamlines and 80 potential lines were created by interpolation from the 50 x 80 uniform mesh generated by the two grid generators and were used in the ADD code flow calculations. The results of these two flow analyses are given in Figs. 15 through 18. A comparison of the calculated results for the static pressure along the inner wall using the two grid generators is given in Fig. 15. A similar comparison for the outer wall is given in Fig. 16. From Fig. 15 it is apparent that the calculation using the new grid generator produces a smoother pressure distribution than that produced by the old grid generator. Otherwise the two analyses have nearly identical pressure distributions along the inner wall. It should be noted that the drop in pressure from $Z/\ell = 0.6$ to $Z/\ell = 2.0$ is due to the exit guide vane (EGV) blockage. A comparison of the skin friction, C_f, along the inner and outer walls are shown in Figs. 17 and 18, respectively, for the two grid generators. The large jump in the friction coefficient $Z/\ell = 0.6$ is also produced by the EGV strut leading edge influence. The "kinks" observed in the skin friction are produced by the rapid increase in skin friction produced by the strut leading edge and subsequent adjustments of the flow. These "kinks" can be removed by a finer grid.

The following conclusions were reached for this evaluation of the two grid generation procedures: (1) the computation time is approximately the same using either method, (2) both methods produce nearly identical metric coefficients except that the Davis method produces smoother metric coefficients in regions of large curvatures, and (3) the Davis method is an improvement over the Anderson method and thus was incorporated into the ADD code for use in the present investigations.

4.2 AGT101 Turbine Inlet Duct

The viscous turbulent flow through the AGT101 turbine inlet duct, with struts, was calculated using inlet flow conditions supplied by NASA-Lewis Research Center. The computational mesh and geometry used to represent the AGT101 turbine inlet duct in the ADD code analysis is shown on Fig. 19. This turbine inlet duct is a transition duct from the combustor exit plane to the turbine inlet plane and contains three struts arranged circumferentially around the duct. The plane view of these struts is shown in Fig. 19. The blunt stagnation point at the axis of symmetry is replaced by a faired streamline to bypass the need to solve stagnation point flow since the equations used in the ADD code are singular at this point.

The duct wall coordinates were obtained by reading coordinate points directly from an engineering drawing. These input points were then least squares spline smoothed using an existing ADD code option and then interpolated to 100 equally spaced arc length distances along the wall. The three struts were support struts only and had no airfoil designation. Their profile coordinates were obtained from engineering drawings and input into the code using the arbitrary airfoil shape option. The cord, maximum thickness and other geometric properties were also obtained from engineering drawings.

Initial flow conditions specified by NASA personnel were uniform total temperature at 441.3 Kelvin deg and uniform total pressure at 1.47×10^5 N/m^2 with a corrected weight flow of .1528 kg/sec. These conditions are sufficient to set up all flow variables at the initial station which satisfy the global continuity equation, normal momentum equation, and equation of state. The analysis was started downstream of the hub stagnation point to bypass the stagnation point solution. Turbulent boundary layers were assumed and a low Reynolds number turbulence model option available in the ADD code was used. It was found that the Reynolds number per inch was so low that a turbulent boundary layer start using a momentum thickness estimated from a stagnation point solution was not possible. Since a laminar turbulent transition model is not currently available in the ADD code, the initial station was chosen further downstream and the momentum thickness increased. At this initial station, the Reynolds number based on momentum thickness was 400.

A geometric mesh was calculated by the new coordinate generator consisting of 50 equally-spaced streamlines and 100 potential lines. Uniform and absolute convergence of the conformal mapping solution was obtained to a tolerance of 1.5×10^{-4} in 13 iterations. The computational CPU time on a UNIVAC 1100/81A operating system was 29.5 minutes. The computational mesh shown on Fig. 19, consisting of 99 unevenly spaced streamlines and 100 potential lines, was obtained by linear interpolation from the 50 x 100 uniform mesh in order to provide adequate resolution of the flow in the wall boundary layers.

The results of the flow analysis of the AGT101 turbine inlet duct are shown on Figs. 20 and 21. These figures show a comparison of the calculated static pressure along the hub and shroud walls with experimental data. The solid line on Figs. 20 and 21 is the solution obtained from the viscous solver in the ADD code and the dashed line is the solution obtained from the approximate inviscid solver in the ADD code analysis.

From Figs. 20 and 21 it is observed that the results of the viscous solver agree quite well with the experimental data. The close agreement between the results of the viscous solution and the approximate inviscid solution, shown on Figs. 20 and 21 indicate that in this case the effect of blockage due to the boundary layer is very slight except near the maximum duct height. The ADD code viscous solution did not predict separation in the AGT101 turbine inlet duct for the specified flow conditions. The computational CPU time was 11.6 minutes for the complete flow calculation. Of this time, 1.2 minutes was required for the approximate inviscid solution on a 85 x 99 mesh and 10.4 minutes was required for the viscous solution on a 254 x 99 mesh.

The test case demonstrates that the current approach is capable of representing the turbulent flow through a complex duct shape that turns almost 180 degrees and contains struts or guide vanes. Two areas for future enhancement of the approach have been identified. First, it is noted that the laminar to turbulent transition model would be beneficial and second, incorporation of a stagnation point capability would relieve a current approximation used for such inlet geometries.

4.3 AGT101 Turbine Exhaust Diffuser

The performance of the AGT101 turbine exhaust diffuser (see Fig. 22) was measured on a test stand in which the turbine exhaust was simulated using inlet guide vanes. These inlet guide vanes (IGV) were a set of 16 blades with a 27 deg circular arc camber which were used to impart swirl to the flow. The projection of these inlet guide vanes onto the (r,z) plane is shown on Fig. 21. Axial flow enters the inlet guide vanes and leaves with a swirl angle of approximately 27 deg. This swirling flow enters the diffuser at the diffuser inlet station and is turned radially outward to exhaust at the diffuser exit plane.

The computational mesh, shown on Fig. 22, consists of 100 streamlines and 100 streamwise stations where the streamlines are packed near each wall to provide grid resolution for the boundary layer calculation. This computational mesh was interpolated from a 50 x 100 uniform mesh which was calculated using the algorithm described in Sect. 3.1. Computational time on the Univac 1100/81A computer was approximately 15 min. to obtain a convergence level of 10^{-4}.

Inlet conditions provided by NASA consisted of uniform total pressure and temperature at standard atmospheric conditions. A corrected weight flow (.667 kg/sec) was provided to set the inlet Mach number. However, this weight flow established a Mach number at the IGV exit plane which was not consistant with the measured wall static to total pressure ratio. A guess for the actual weight flow (.789 kg/sec) was made in an attempt to establish the correct initial conditions. In actual practice the weight flow should be established by the ambient pressure at the diffuser exit.

An overall view of the solution for the flow through exhaust diffuser is shown on Fig. 23. This is a plot of the streamwise velocity distribution across the duct at successive streamwise stations. The boundary layer growth on the hub and shroud walls is vividly illustrated. On the hub wall the boundary layer grows slowly as the flow is decelerated by the initial portion of the turn. Then the boundary layer thickness decreases as it recovers from the turn. Finally the boundary layer grows slowly as it is decelerated in the radial diffuser. On the shroud wall, the boundary layer is initially accelerated as the flow enters the turn. Then the boundary layer grows rapidly as the flow recovers from the turn and continues to decelerate in the radial diffuser. At the exit, the shroud boundary layer is nearly separated and occupies almost one half the exit flow. The corresponding behavior of the wall friction coefficient is shown on Fig. 24 and is consistent with the varying streamwise pressure distribution. In particular it is noted that near the exit, the shroud boundary layer is nearly separated.

A more detailed plot of the calculated flow field is shown on Figs. 25 and 26. Fig. 25 shows a comparison of the inlet and exit streamwise velocity profiles. At the inlet, the flow is uniform with thin boundary layers. At the exit, the shroud wall shows a large nearly separated boundary layer. The flow angles at the IGV trailing edge and at the diffuser exit are shown on Fig. 26. At the IGV trailing edge, the core flow outside the boundary layer has a flow angle varying from approximately 28 deg down to approximately 18 degrees. Inside the hub boundary layer the flow angle increases rapidly to almost 50 deg. and inside the shroud boundary layer the flow angle increases to approximately 30 deg. This increase in flow angle in the wall boundary layers is known as "flow overturning" and is a well known phenomena predicted by secondary flow theory (see Refs. 44 through 50). The flow angle distribution at the exit is more interesting however. Through the hub boundary layer and the core flow, the flow angle has been reduced to less than 10 deg. This is caused by conservation of angular momentum. As the swirling flow moves outward in the radial diffuser, its tangential velocity must be correspondingly reduced. In the shroud boundary layer, however, the flow angle increases to nearly 90 deg. This is caused by the nearly separated streamwise boundary layer. At separation the flow angle would be 90 deg. because the streamwise component of stress is zero while the tangential component of stress is finite.

A comparison of the calculated wall pressure distribution with the measured pressured distribution on both the hub and shroud walls is shown on Fig. 27. The agreement with experimental data is quite good considering the complexity of the flow field and the approximations necessary for estimating weight flow and IGV performance characteristics. The overall flow is quite involved and can be explained in the following manner. At the inlet upstream of the IGV, the flow is uniform so that the hub and shroud static pressures are the same. Downstream of the inlet guide vane, the flow is swirling and normally the shroud static pressure should be greater than the hub pressure to establish radial equilibrium. However because the flow is starting to turn, an opposing pressure gradient over comes that set-up by the swirling flow. Through the turn, the hub static pressure is greater than the shroud pressure. In the radial diffuser, the static pressures are nearly the same. (note that the surface length differs on the two walls.) This pressure history clearly shows why the shroud boundary layer is nearly separated while the hub boundary layer is not.

Effects to be examined more closely are: 1) free stream turbulence and the results from using different turbulence models (Ref. 8), 2) axisymmetric streamline curvature corrections as developed in (Ref. 8), and 3) nonaxisymmetric mixing effects such as those described in Ref. 51.

5.0 CONCLUSION AND RECOMMENDATIONS

A new coordinate generator based on the work of Davis (Ref. 9) has been incorporated into the ADD code and has been shown capable of calculating coordinates for small gas turbine ducts which turn more than 90 degrees. This new coordinate generator has been shown to produce improved results over the previous grid generator developed by Anderson (Ref. 1). Turbulent viscous flow calculations have been demonstrated for small gas turbine ducts with struts and guide vanes using a generalized strut geometry and blade force calculation procedure. The computed results for pressure distribution compare favorably with experimental data.

A literature survey on calculation procedures used in gas turbine technology has demonstrated compatability with the ADD code formulation and has indicated several areas for future improvement. These areas are 1) incorporation of a secondary flow mixing model to account for three dimensional effects due to corner flow and tip leakage and 2) development of a blade force calculation procedure for radial flow turbines and compressors. The calculated test cases also indicate that a laminar turbulent transition model and stagnation point solution would be useful.

6.0 REFERENCES

1. Anderson, O. L.: Calculation of Internal Viscous Flows in Axisymmetric Ducts at Moderate to High Reynolds Numbers, Int. J. of Computers and Fluids, Vol. 8, No. 2, June 1980.

2. Anderson, O. L.: User's Manual for a Finite Difference Calculation of Turbulent Swirling Flow in Axisymmetric Ducts with Slot Cooled Walls, Vol. I & II, USAAMRDL-TR-50, 1974.

3. Bowditch, D. N.: Some Design Considerations for Supersonic Cruise Mixed Compression Inlets, AIAA/SAE 9th Propulsion Conference AIAA Paper No. 73-1269, Nov. 1973.

4. Povinelli, L. A.: An Experimental and Analytical Investigation of Axisymmetric Diffusers, AIAA J. Vol. 14, No. 9, 1976, P. 1280.

5. Anderson, O. L.: A Comparison of Theory and Experiment for Incompressible Turbulent Swirling Flows in Axisymmetric Ducts, AIAA 10th Aerospace Sciences Meeting, AIAA Paper No. 72-43, Jan. 1972.

6. Barber, T. J., P. Raghuraman, and O. Anderson: Evaluation of an Analysis for Axisymmetric Internal Flows in Turbomachinery Ducts, Flow in Primary Non-Rotating Passages in Turbomachines, ASME Winter Annual Meeting, Dec. 1979.

7. McLallin, K. L., and M. G. Kofskey: Investigation of the Interstage Duct and Its effect on Power Turbine Performance, Automotive Technology Development Contractor Coordination Meeting, Oct. 1979.

8. Anderson, O. L., and D. E. Edwards: Extensions to an Analysis of Turbulent Swirling Compressible Flow in Axisymmetric Ducts, UTRC Report R81-914720-18, Feb. 1981.

9. Davis, R. T.: Numerical Methods for Coordinate Generation Based on Schwartz-Christoffel Transformation, AIAA Paper No. 79-1463, 4th Computational Fluid Dynamics Conference, July 1979.

10. Sridhar, K. P., and R. T. Davis: A Schwartz-Christoffel Method for Generating Internal Flow Grids. To be presented at ASME 102 Winter Annual Meeting, Nov. 1981.

REFERENCES (Cont'd)

11. Johnson, I. A., and R. O. Bullock: Aerodynamic Design of Axial Flow Compressors, NASA SP36, 1965.

12. Abbott, I. H., and A. E. VonDoenhoff: Theory of Wing Sections, Dover Pub., 1959.

13. Hanley, W. T.: A Correlation of End Wall Losses in a Plane Compressor Cascade, ASME Jr. Eng. for Power, July 1968, pp. 251-257.

14. Papailiou, K. D., R. Flot, and J. Mathieu: Secondary Flows in Compressor Bladings, ASME J. of Eng. for Power, Vol. 99, April 1977, pp. 211-224.

15. Koch, C. C., and L. H. Smith: Loss Sources and Magnitudes in Axial Flow Compressors, ASME Paper No. 75 WA/GT-6, ASME J. Eng. for Power, Vol. 98, No. 3, July 1976, p. 411.

16. Squire, H. T., and K. G. Winter: The Secondary Flow in a Cascade of Aerofoils in a Nonuniform Stream, J. of Aeronautical Sciences, Vol. 18, 1951.

17. Coles, D.: The Law of the Wake in the Turbulent Boundary Layer, Jr. of Fluid Mechanics, Vol. 1, Part 2, July 1956, pp. 191-226.

18. Mager, A., J. J. Mahoney and R. E. Budinger: Discussion of Boundary Layer Characteristics Near the Wall of an Axial Flow Compressor, NACA Report 1085, 1951.

19. Schlicting, H.: Boundary Layer Theory, McGraw Hill Book Co., Inc. New York, 1955.

20. Dring, R. P., L. W. Hardin, H. D. Joslyn and J. H. Wagner: Research on Turbine Rotor-Stator Aerodynamic Interaction and Rotor Negative Incidence Stall, UTRC Report R81-915048, November 1981.

21. Wu, C. H.: A General Theory of Three-Dimensional Flow in Subsonic and Supersonic Turbomachines of Axial Radial and Mixed Types. NACA TN 2604, 1952.

22. Marsh, H.: A Digital Computer Program for the Through-Flow Fluid Mechanics in an Arbitrary Turbomary Using a Matrix Method Aeronautical Research Council R&M No. 3509, 1968.

23. Wu, C. H.: Application of Radial-Equilibrium Condition to Axial Flow Compressor and Turbine Design, NACA TR 955 1949.

REFERENCES (Cont'd)

24. Mellor, G. L.: Reconsideration of the Annulus Flow Problem in Axial Flow Turbomachiner, Trans. ASME Series D, Vol. 84, 1962, pp. 579-589.

25. Smith, L. H.: The Radial Equilibrium Equation for Turbomachinery, ASME J. Eng. for Power, Series A, Vol. 88, No. 1, January 1966, pp. 1-12.

26. Novak, R. A.: Streamline Curvature Computing Procedures for Fluid Mechanics, ASME J. of Engineer for Power, October 1967.

27. Railly, J. W., and J. H. G. Howard: Velocity Profile Development in Axial Flow Compressors, Jr. Mech. Eng. Science, Vol. 4, 1962.

28. Mellor, G. L., and G. M. Wood: An Axial Compressor End-Wall Boundary Layer Theory, ASME Jr. Basic Eng., Vol. 93, June 1971, pp. 300-316.

29. Horlock, J. H., and H. J. Perkins: Annulus Wall Boundary Layers in Turbomachines, AGARDograph, No. 185, May 1974.

30. Marsh, H., and J. H. Horlock: Wall Boundary Layers in Turbomachines, Jr. Mech. Eng. Science, Vol. 14, No. 6, 1972, pp. 411-423.

31. Daneshyar, M., J. H. Horlock, and H. Marsh: Prediction of Annulus Wall Boundary Layers in Axial Flow Turbomachines, AGARDograph, No. 164, April 1972.

32. DeRuyck, J., and C. Hirsch: Investigations of an Axial Compressor End-Wall Boundary Layer Prediction Method, ASME Paper No. 80-GT-53, March 1980.

33. DeRuyck, J., C. Hirsch, and P. Kool: An Axial Compressor End-Wall Boundary Layer Calculation Method, ASME Jr. of Eng. for Power, Vol. 101, No. 2, 1979. pp. 223-249.

34. DeRuyck, J., C. Hirsch, and P. Kool: Investigation on Axial Compressor End-Wall Boundary-Layer Wall Calculations, Intl. Joint Gas Turbine Congress and Exhibition, Israel, 1979.

35. Hirsch, C.: Flow Prediction in Axial Flow Compressors Including End-Wall Boundary Layers, ASME Jr. of Eng. for Power, Vol. 96, 1974, pp. 413-426.

36. Hirsch, C.: End-Wall Boundary Layers in Axial Compressors, ASME Paper No. 76-GT-72, 1976.

37. Comte, A., G. Ohayon, and K. D. Papailiou: A Method for the Calculation of the Wall Layers Inside the Passage of a Compressor Cascade With and Without Tip Clearance, ASME Paper No. 81-GT-168, March 1981.

REFERENCES (Cont'd)

38. Papailiou, K. D.: Boundary Layer Optimization for the Design of High Turing Axial Flow Compressor Blades, ASME Jr. of Eng. of Power, Vol. 93, January 1971, pp. 147-155.

39. Assassa, G., and K. D. Papailiou: An Integral Method of Turbulent Boundary Layer with Separation, Jr. Fluids Eng., Vol. 101, No. 1, March 1979, pp. 110-116.

40. Papailiou, K. D.: Correlations Concerning the Process of Flow Deceleration, ASME Paper No. 74-GT-87, 1974.

41. Mellor, G. L., and R. E. Strong: End-Wall Effects in Axial Compressors, ASME Paper No. 67-Fe-16, May 1967.

42. Mellor, G. L., and T. F. Balsa: The Prediction of Axial Compressor Performance with Emphasis on the Effect of Annulus Wall Boundary Layers, AGARDograph, No. 164, 1972, pp. 363-378.

43. Lakshminarayana, B.: Methods of Predicting the Tip Clearance Effects in Axial Flow Turbomachinery, Jr. Basic Eng., September 1970, pp. 467-482.

44. Hawthorn, W. R.: Secondary Circulation in Fluid Flow, Proc. of the Royal Society, Vol. A206, 1951, pp. 374-387.

45. Hawthorn, W. R.: Rotational Flow Through Cascades, Part I - The Components of Vorticity, Quarterly Jr. of Mechanical and Applied Mathematics, Vol. 8, 1955.

46. Hawthorn, W. R., and W. D. Armstrong: Rotational Flow Through Cascades, Part II - The Circulation About the Cascade, Quarterly Jr. of Mechanical and Applied Mathematics, Vol. 8, 1955, pp. 290-292.

47. Hawthorn, W. R.: The Applicability of Secondary Flow Analysis to the Solution of Internal Flow Problem, Fluid Mechanics of Internal Flow, Ed. G. Souran, Elsevier Press, 1967, pp. 238-269.

48. Lakshminarayana, B., and J. H. Horlock: Effects of Shear Flows on the Outlet Angle in Axial Compressor Cascades; Methods of Prediction and Correlation with Experiments, ASME Jr. of Basic Eng., Vol. 89, 1967, pp. 191-200.

49. Horlock, J. H., J. F. Louis, P. M. E. Percival, and B. Lakshminarayana: Wall Stall in Compressor Cascades, ASME Jr. of Basic Eng., September 1966, pp. 639-648.

50. Smith, L. H.: Secondary Flow in Axial Flow Turbomachinery, Trans. ASME, Vol. 77, October 1955, pp. 1065-1076.

REFERENCES (Cont'd)

51. Adkins, G. G., and L. H. Smith: Spanwise Mixing in Axial-Flow Turbomachines, ASME Paper No. 81-GT-57, 1981.

52. Roberts, G. O.: Computational Meshes for Boundary Layer Problems, Proceedings of the Second Intl. Conference on Numerical Methods in Fluid Dynamics, Berlin, Springer-Verlag, 1971, pp. 177-178.

7.0 LIST OF SYMBOLS

b_i	Poles in Schwartz-Christoffel transformation
c	Blade chord (m, ft)
C_f	Friction coefficient
h	Metric coefficient (m, ft)
H	Duct height (m, ft)
H	Shape factor δ^*/θ
i	$\sqrt{-1}$
$\vec{i},\vec{k}$	Unit vectors
M	Rotational constant Schwartz-Christoffel transformation
n,s,ϕ	ADD code coordinates
P_T	Total pressure (n/m^2, lbf/ft^2)
r,z,ϕ	Cylindrical coordinates
Re_θ	Reynolds number based on momentum thickness
t = s+in	Complex variable in t plane, complex potential
t	Blade thickness (m, ft)
u,v	Potential flow velocities (m/sec, ft/sec)
$\vec{u},\vec{v}$	Velocity vectors (m/sec, ft/sec)
U	Magnitude of viscous flow velocity (m/sec, ft/sec)
U_s	Streamwise velocity (m/sec, ft/sec)
V	Magnitude of potential flow velocity (m/sec, ft/sec)

LIST OF SYMBOLS (Cont'd)

x,y,ϕ	Blade coordinates
x_s	Arc length along coordinate s (m, ft)
y	Distance from wall (m, ft)
$z = x+iy$	Complex variable in z plane (duct plane)
Z_{EW}	End wall loss coefficient
α_i	Schwartz-Christoffel wall angle
α_e	Duct exit divergence angle (deg)
α_s	Cascade stagger angle (deg)
δ	Boundary layer thickness (m, ft)
δ^*	Displacement thickness (m, ft)
ε	Error
ε_c	Closure error
$\zeta = \xi+i\eta$	Complex variable in ζ plane
θ	Angle with respect to real axis (deg.)
Θ	Momentum thickness
κ	Streamline curvature (1/m, 1/ft)
μ	Viscosity
ρ	Density (kg/m^3, $slugs/ft^3$)
$\bar{\bar{\sigma}}$	Stress tensor
$\bar{\bar{\tau}}$	Stress tensor
ϕ_c	Circular arc camber (deg)

LIST OF SYMBOLS (Cont'd)

Subscripts

CL	Blade center line
e	Boundary layer edge
J,K	Grid indices
L,U	Lower/upper wall
LI,UI	Intersection lower/upper wall
m	Mean line
1,2	Upstream/downstream station

Superscript

∿	Inviscid flow

8.0 FIGURES

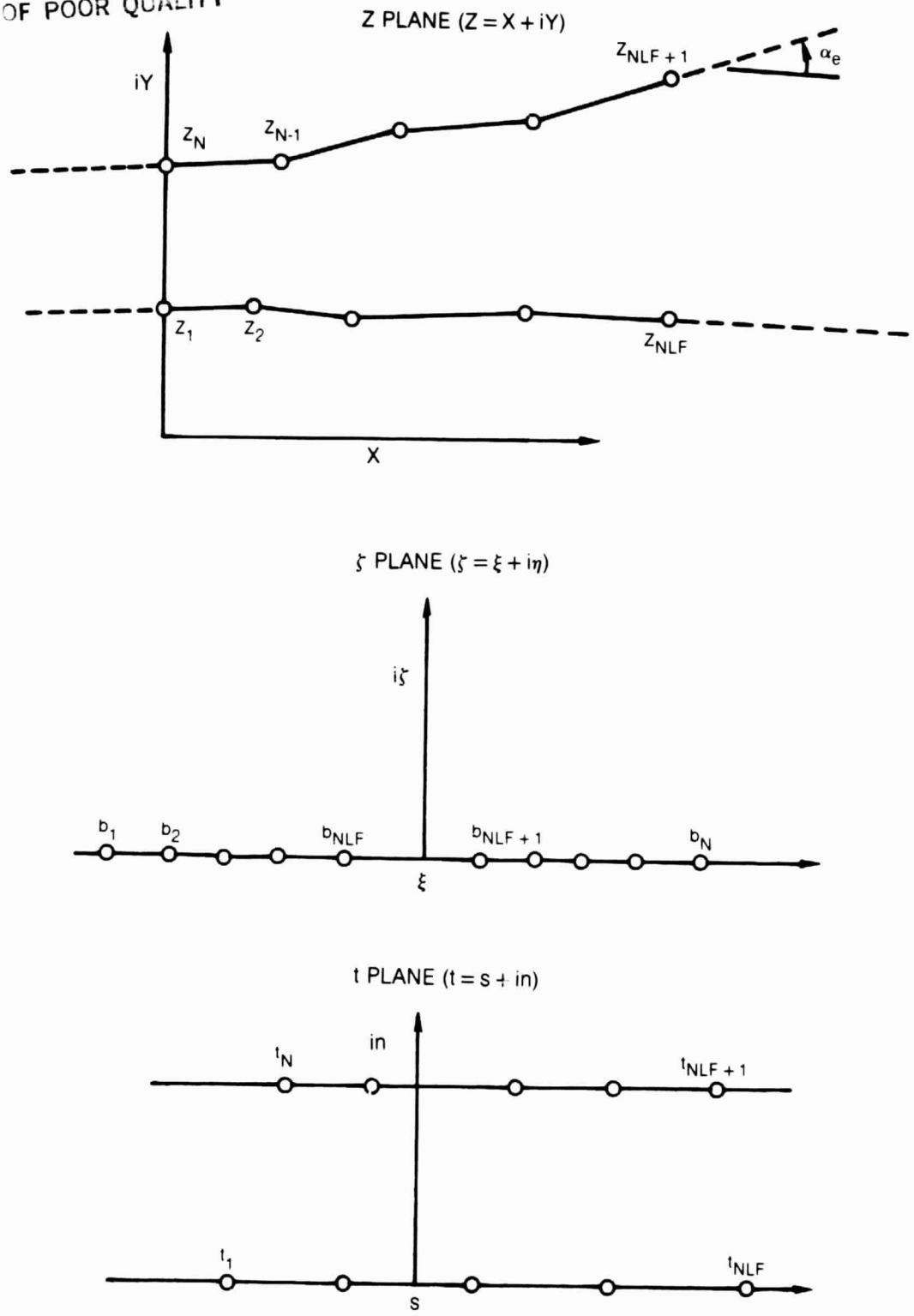

Fig. 1. Mapping of Duct to Straight Channel

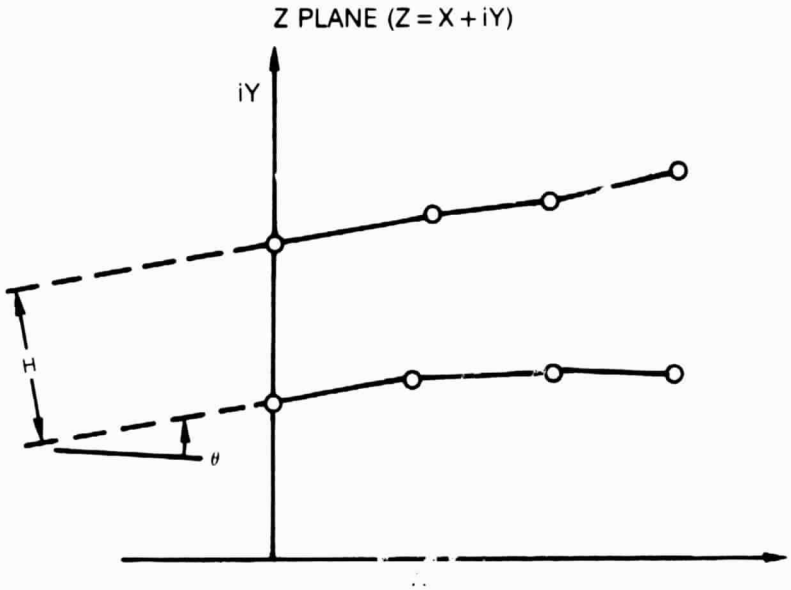

Fig. 2. Asymptotic Solution

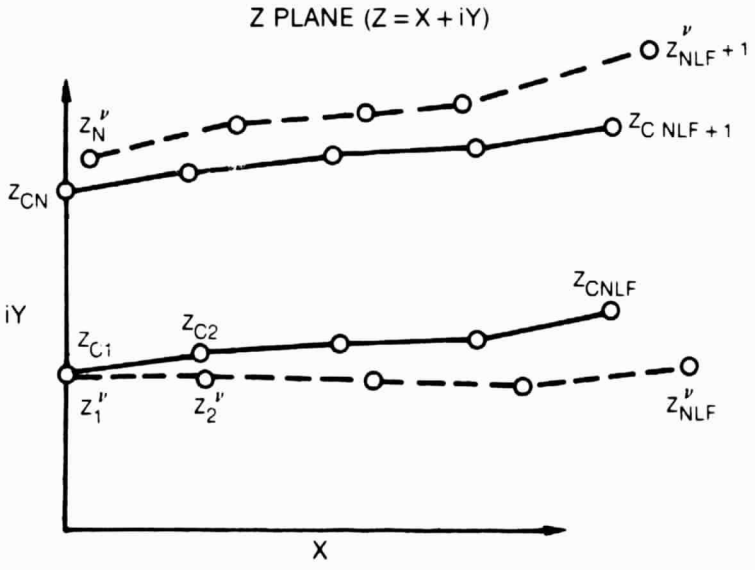

Fig. 3. Integration Update

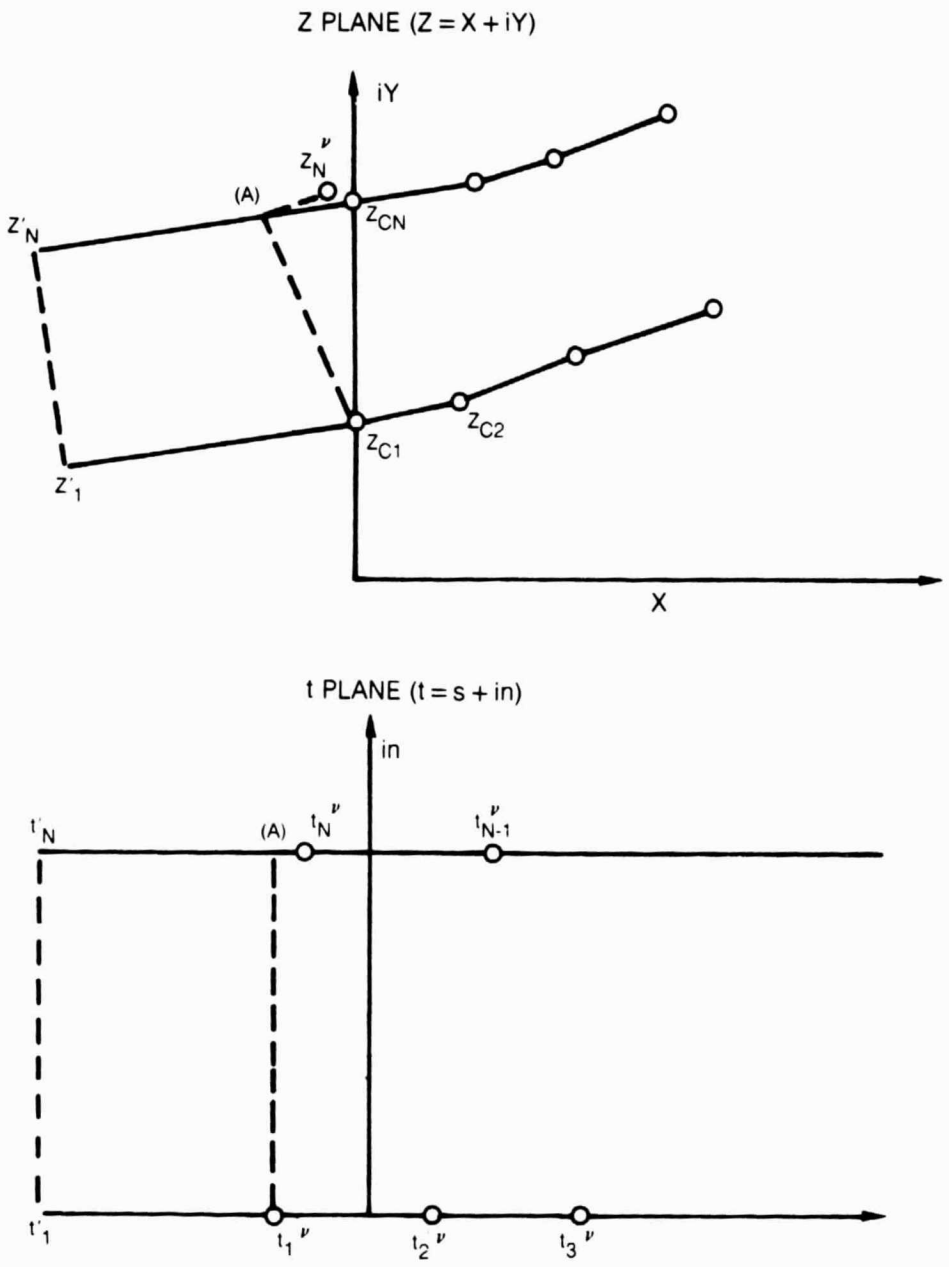

Fig. 4. Update for Corner Point

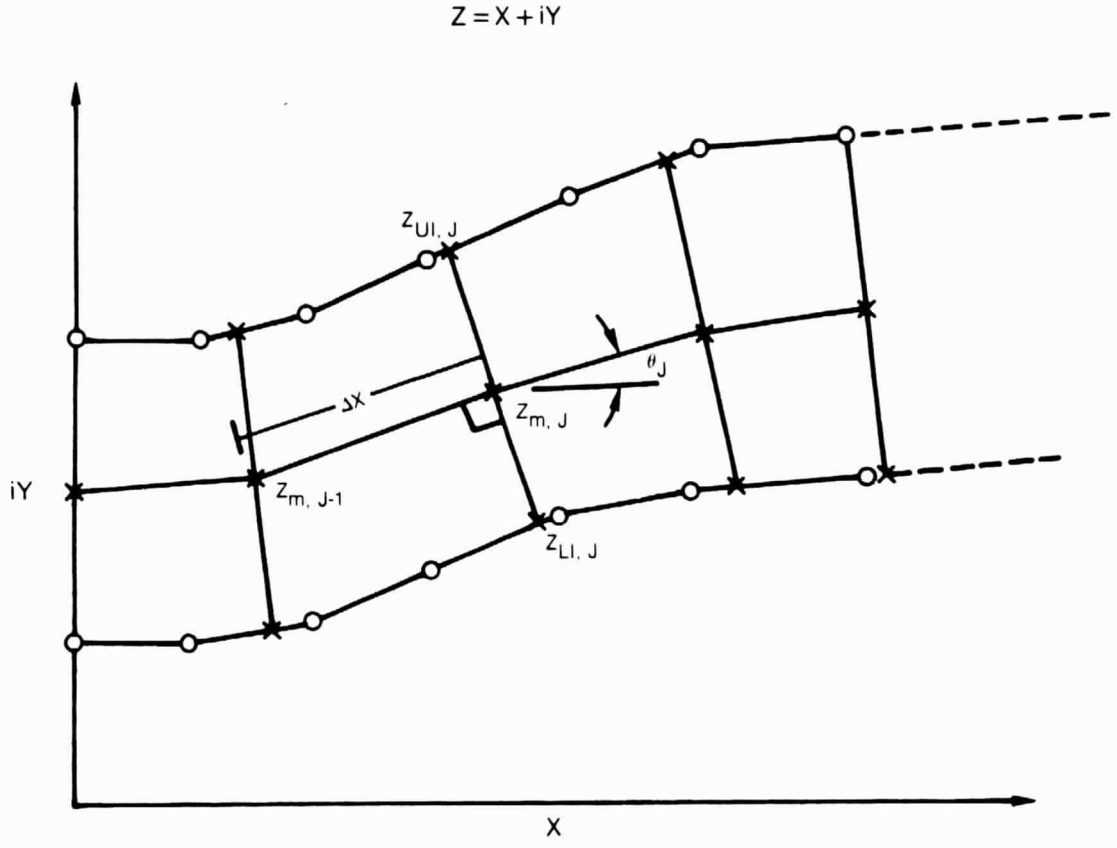

Fig. 5. Geometric Construction of Potential Flow

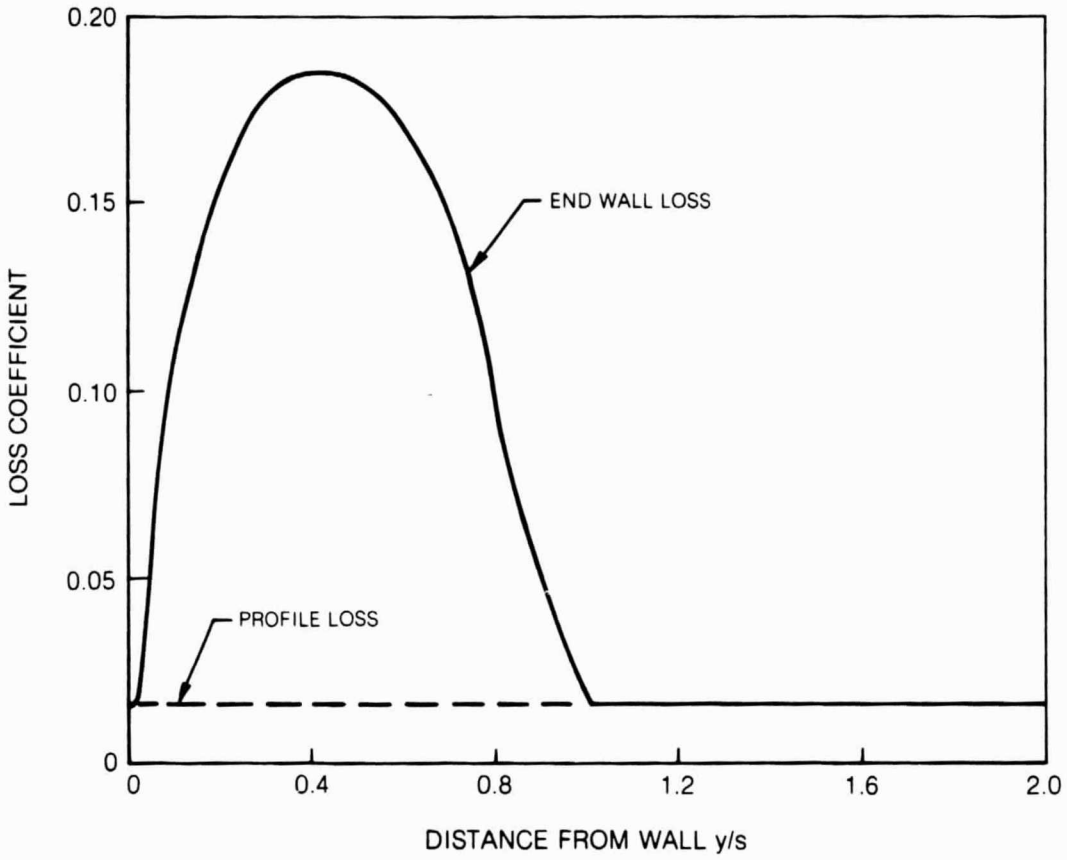

Fig. 6. Comparison of Calculated Profile Loss and End Wall Loss

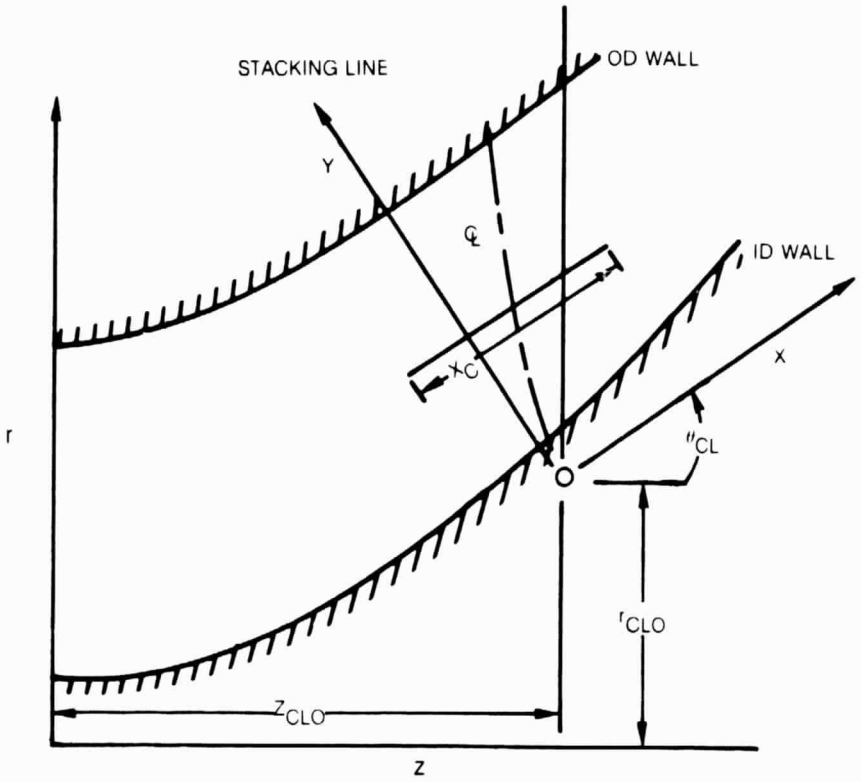

Fig. 7a. Location of Stacking Line

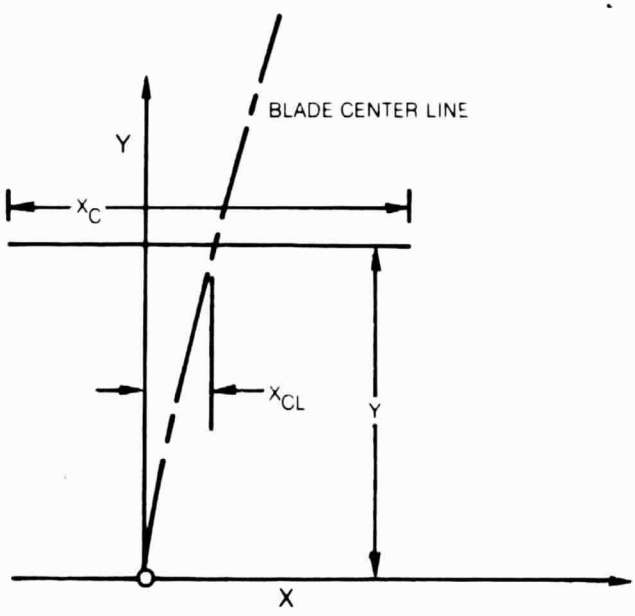

Fig. 7b. Blade Stacking Plane

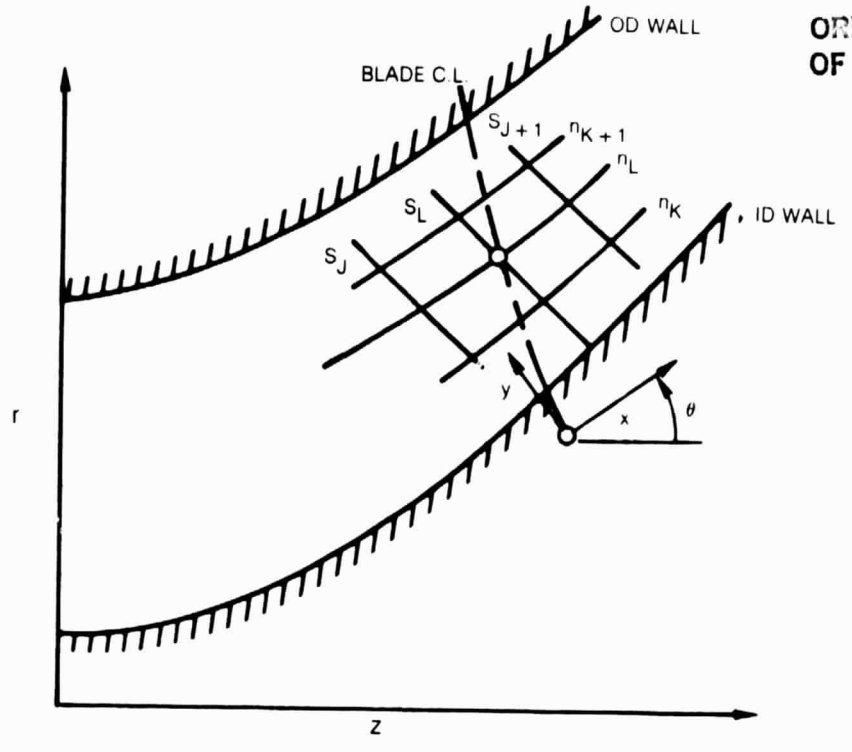

Fig. 8a. Location of Centerline in (n, s) Coordinates

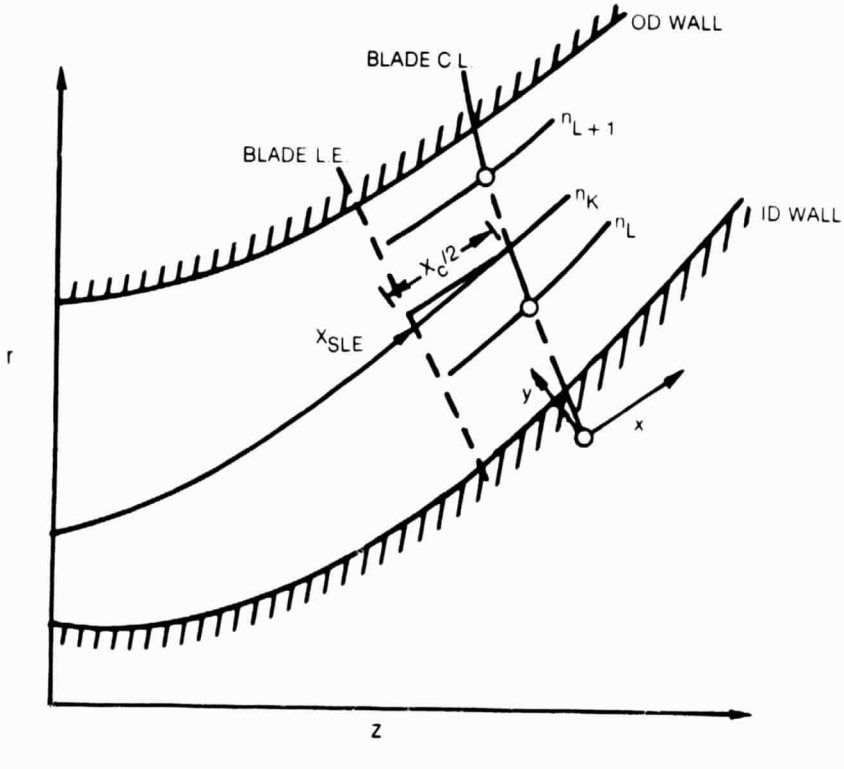

Fig. 8b. Location of Blade Leading Edge

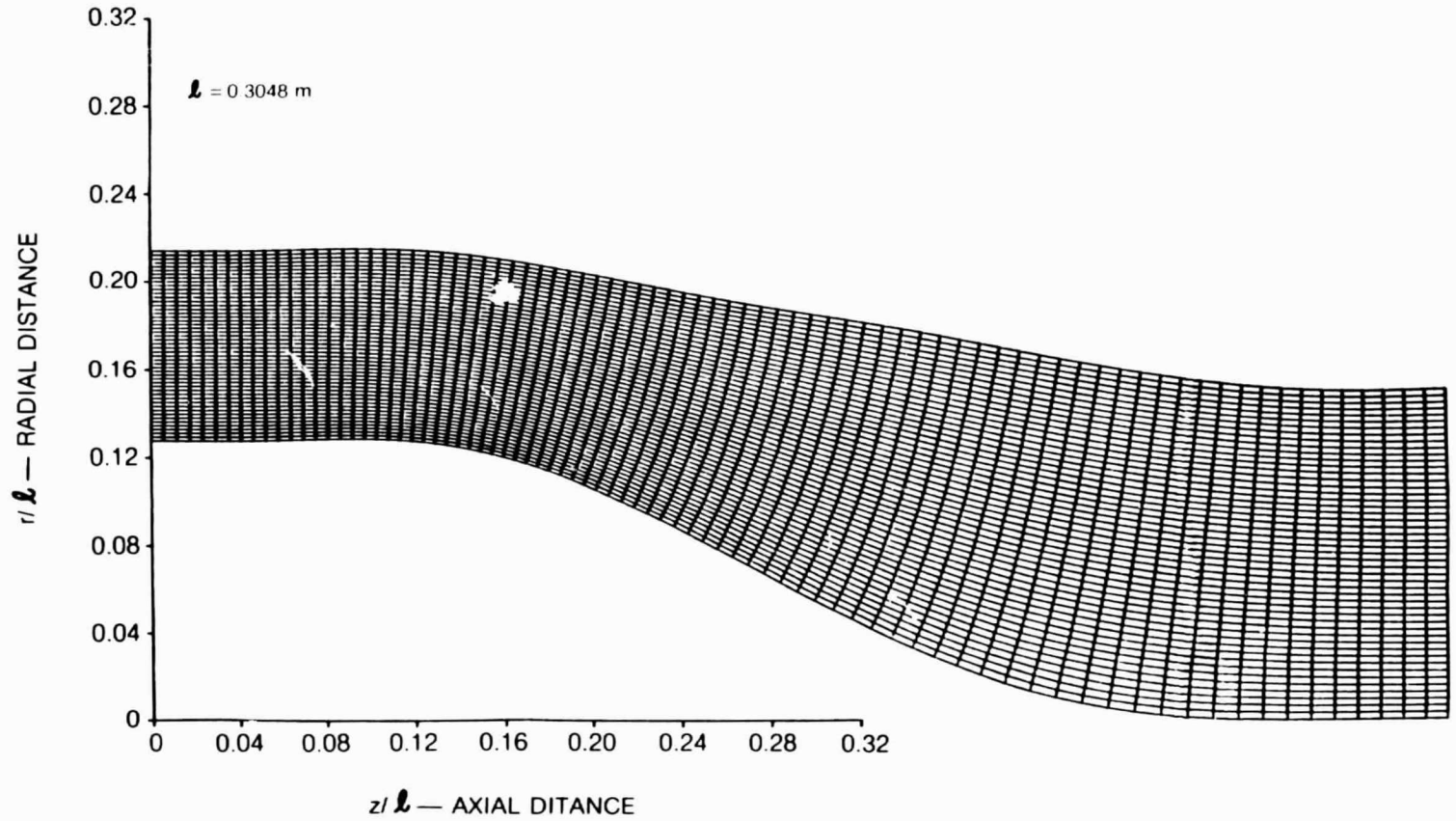

Fig. 9. Geometric Mesh Created By Grid Generator

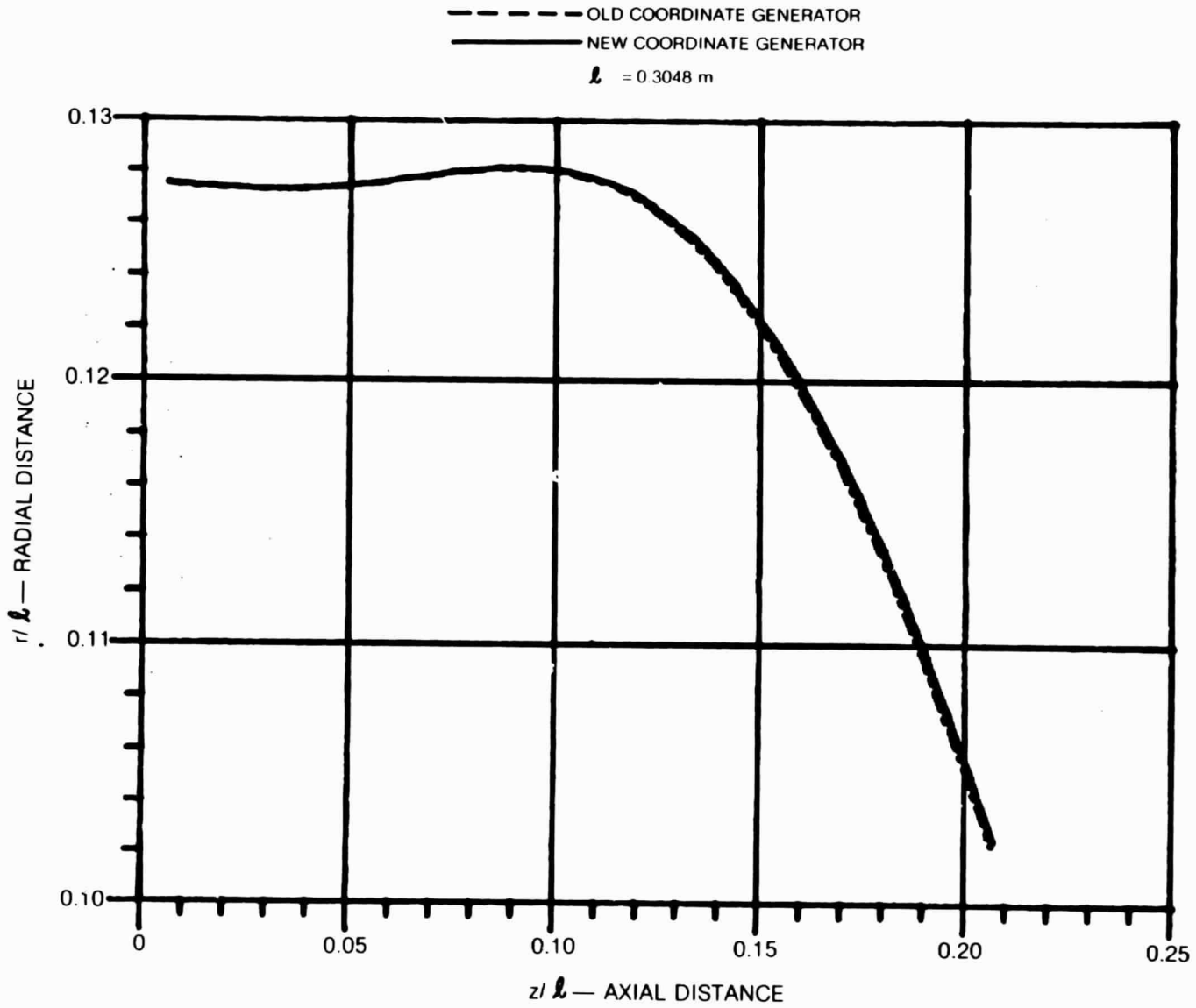

Fig. 10. Comparison of Inner Wall Coordinates Calculated with new and Old Grid Generators

81-10-63-6

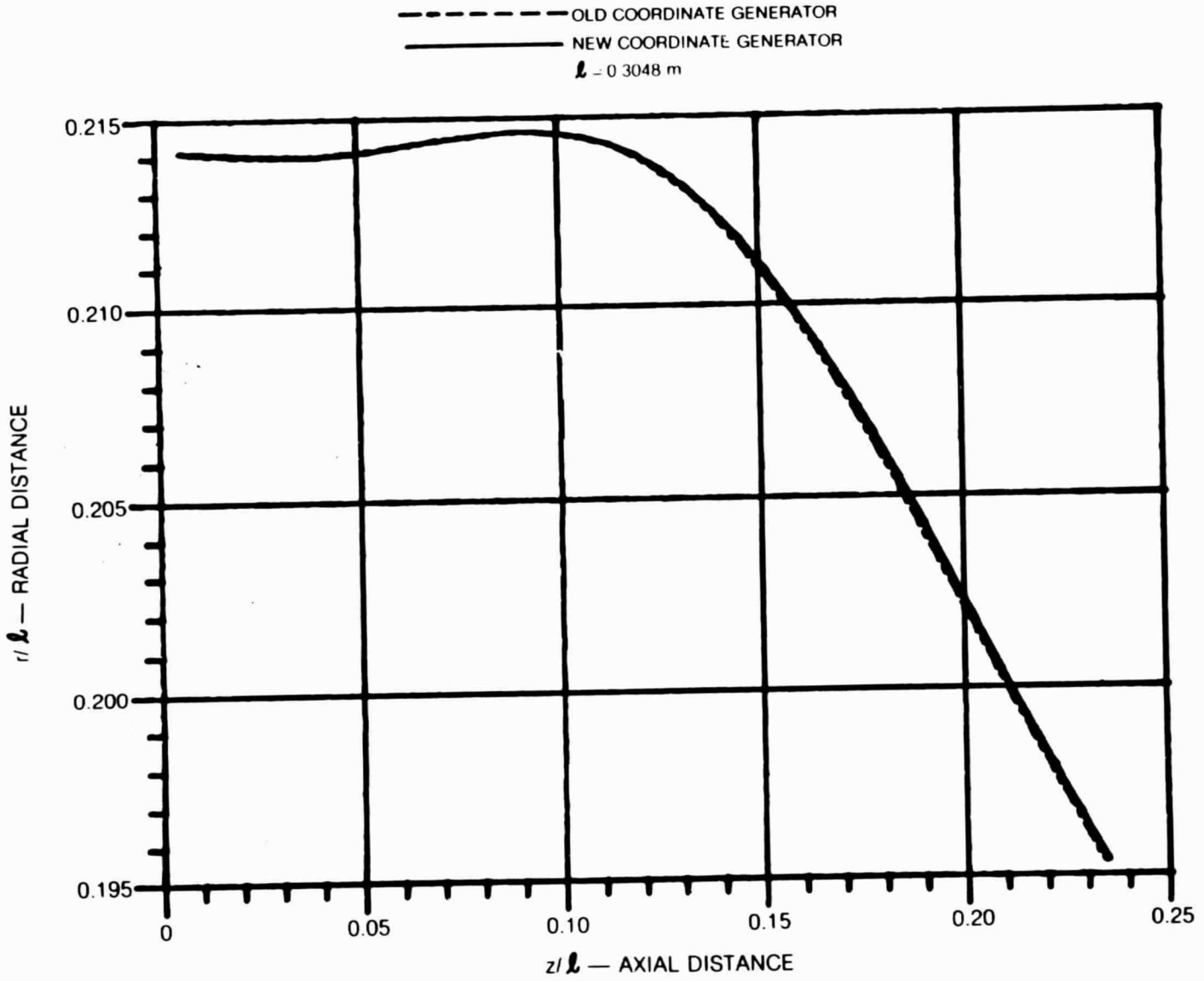

Fig. 11. Comparison of Outer Wall Coordinates Calculated with new and Old Grid Generators

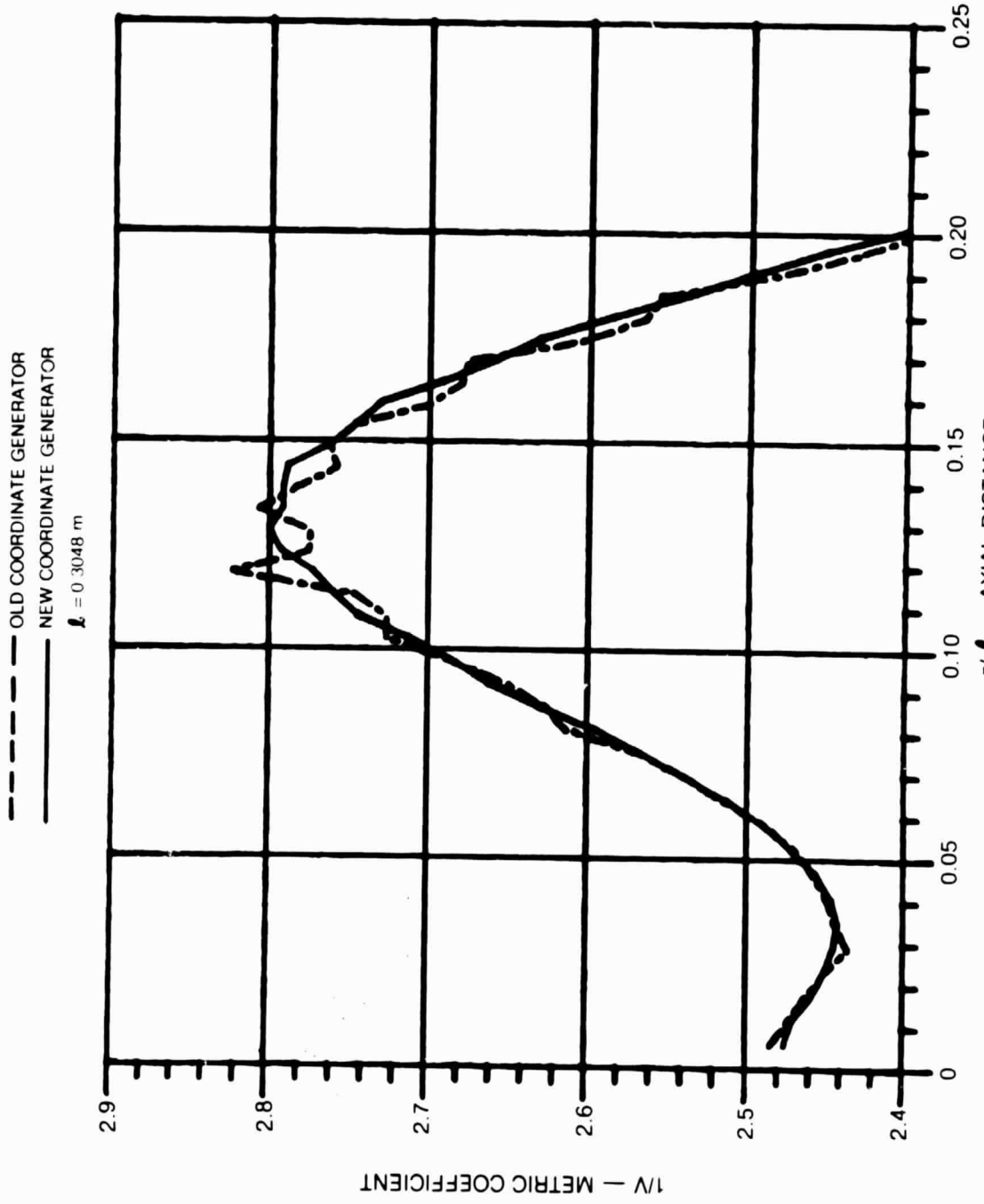

Fig. 12. Comparison of the Inner Wall Metric Coefficient Calculated with New and Old Grid Generators

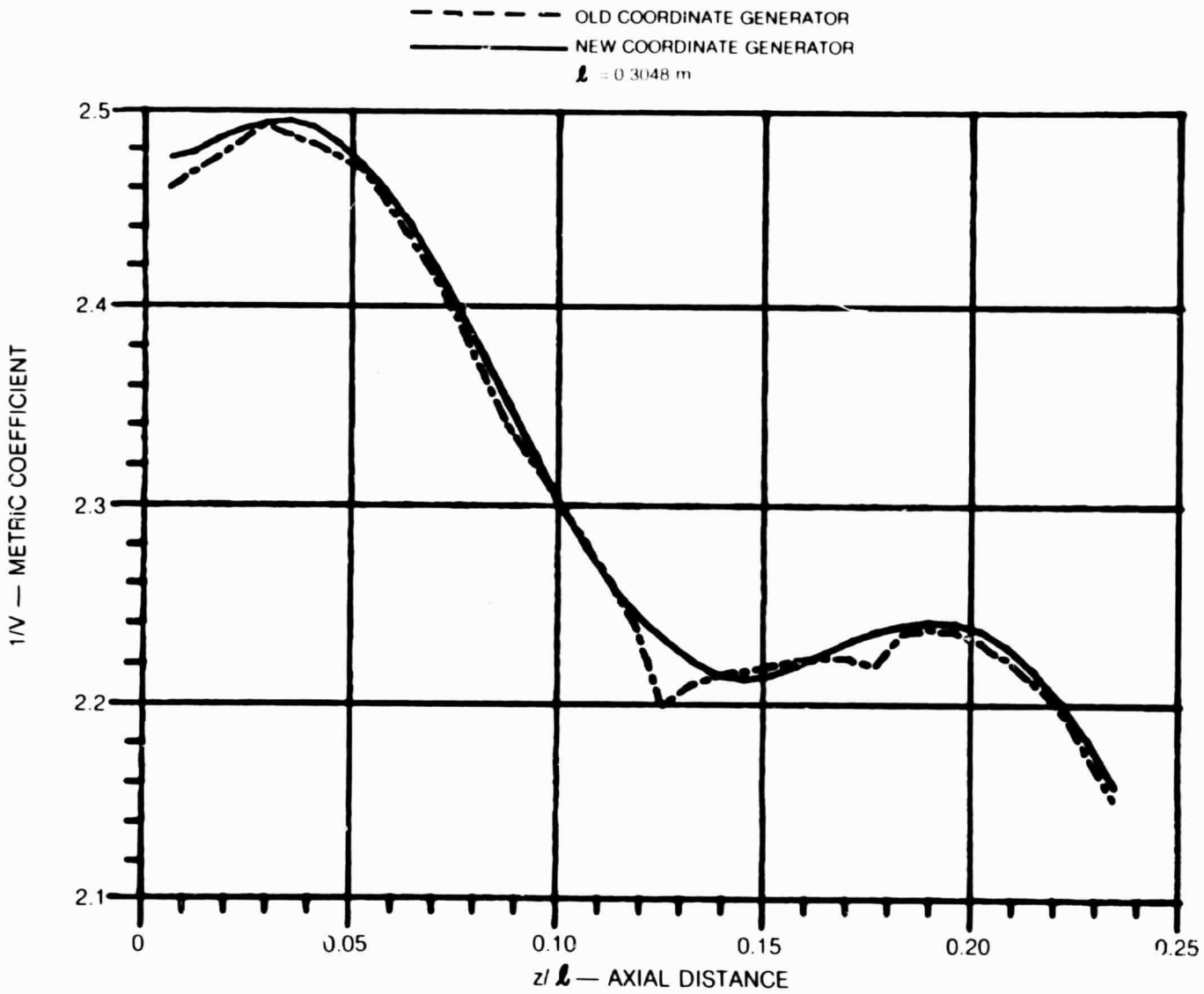

Fig. 13. Comparison of the Outer Wall Metric Coefficient Calculated with New and Old Grid Generators

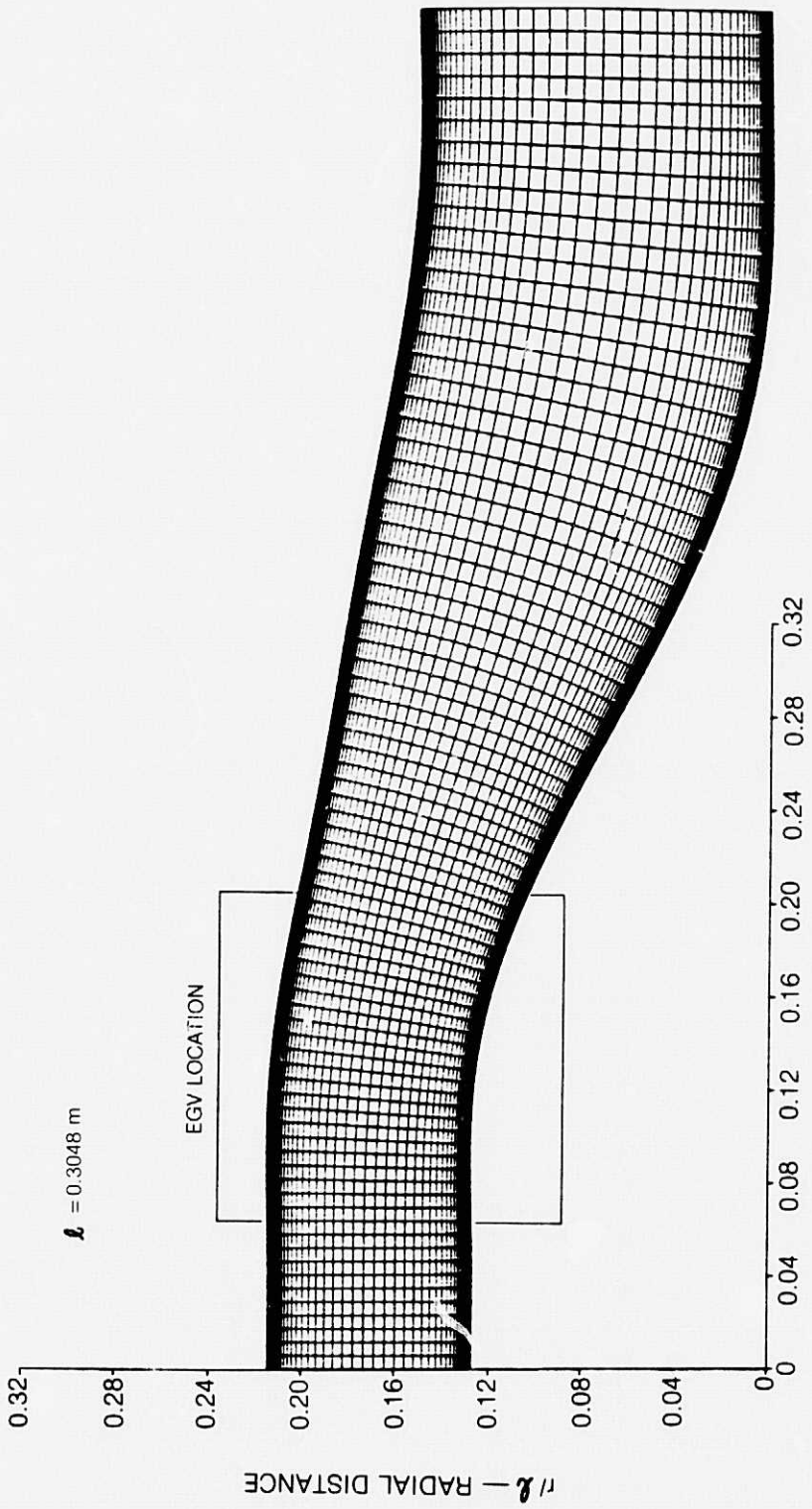

Fig. 14. Numerical Mesh Used In ADD Code Flow Calculation

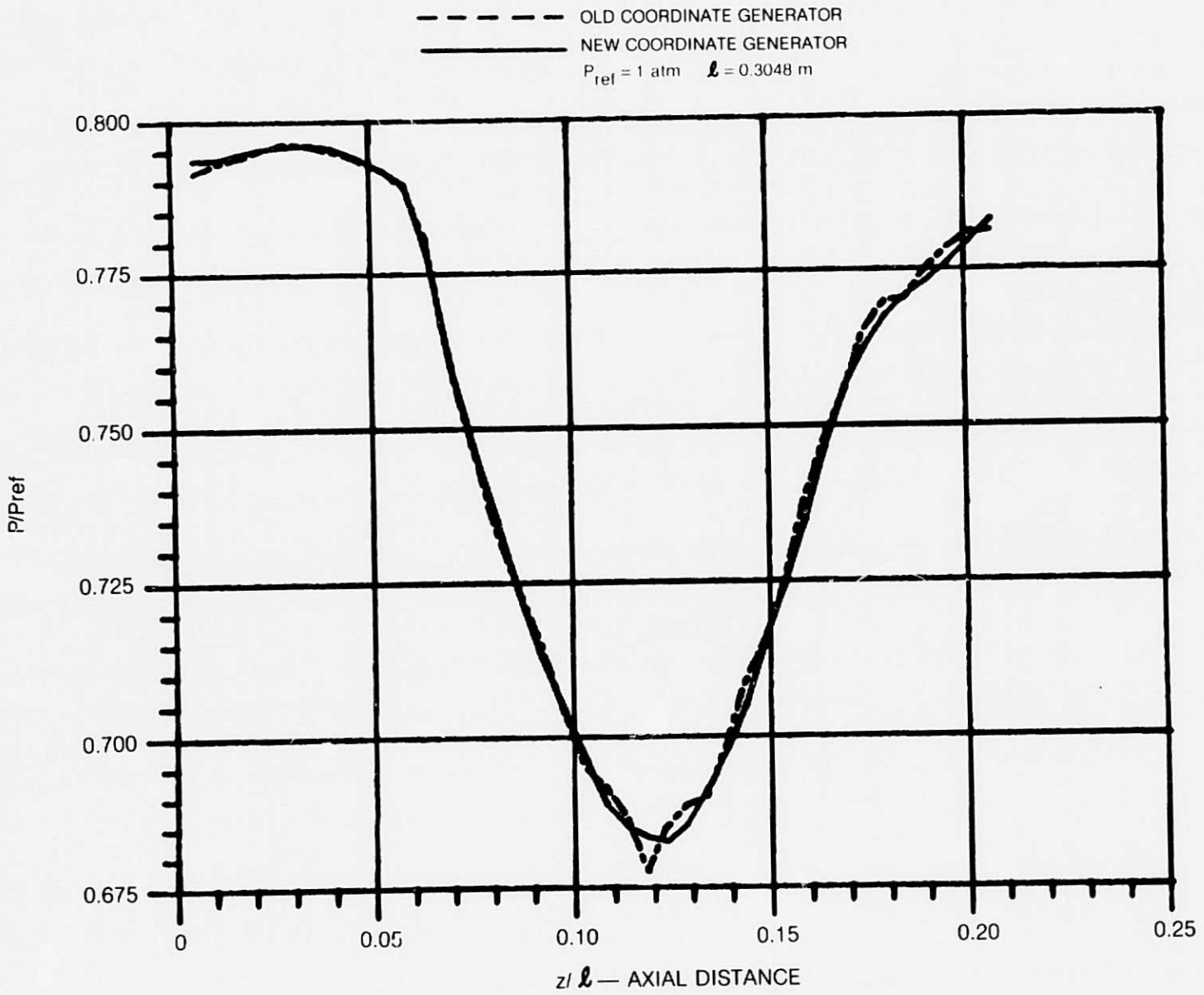

Fig. 15. Comparison of the Inner Wall Static Pressure Calculated with New and Old Grid Generators

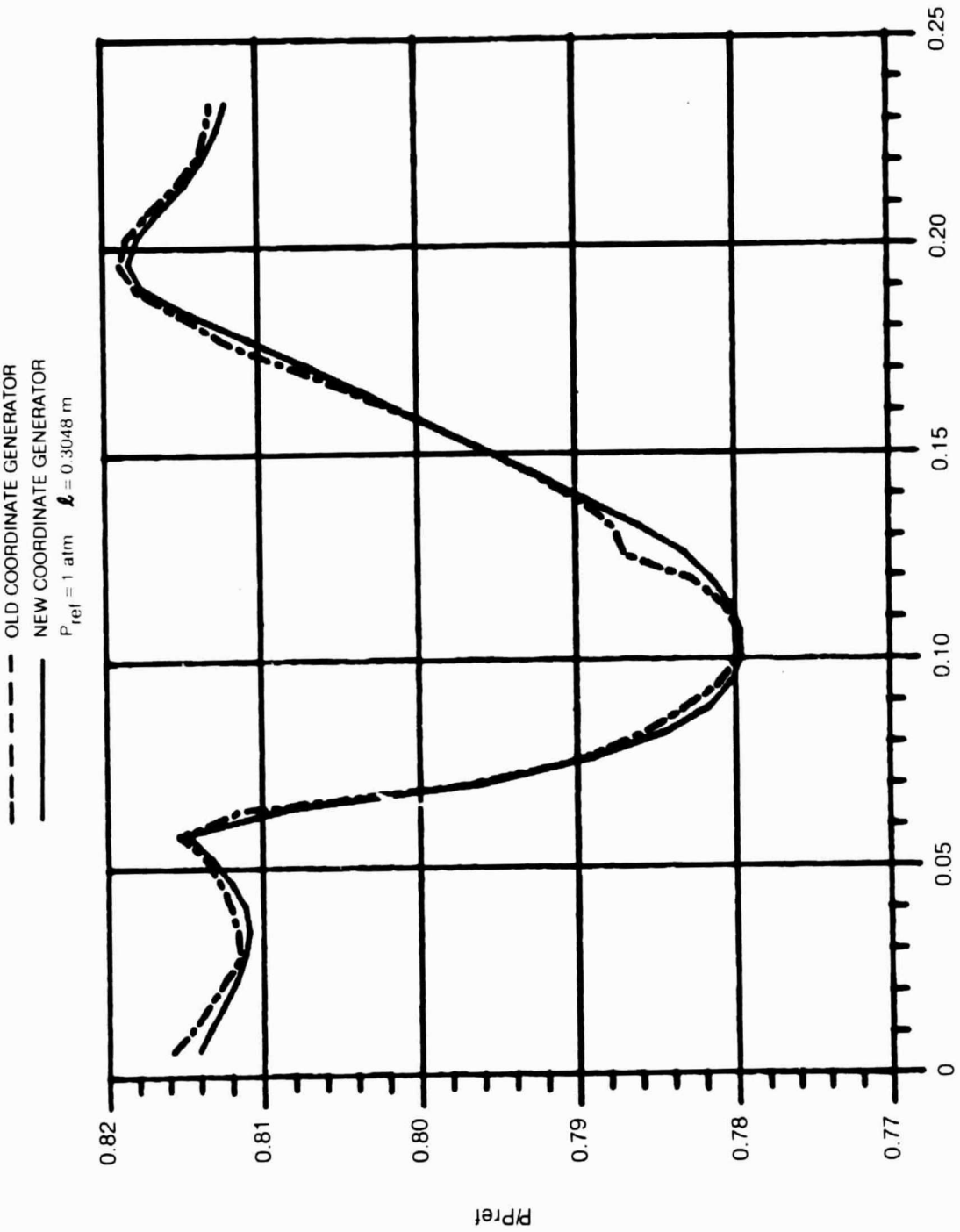

Fig. 16. Comparison of the Outer Wall Static Pressure Calculated with New and Old Grid Generators

81-10-63-12

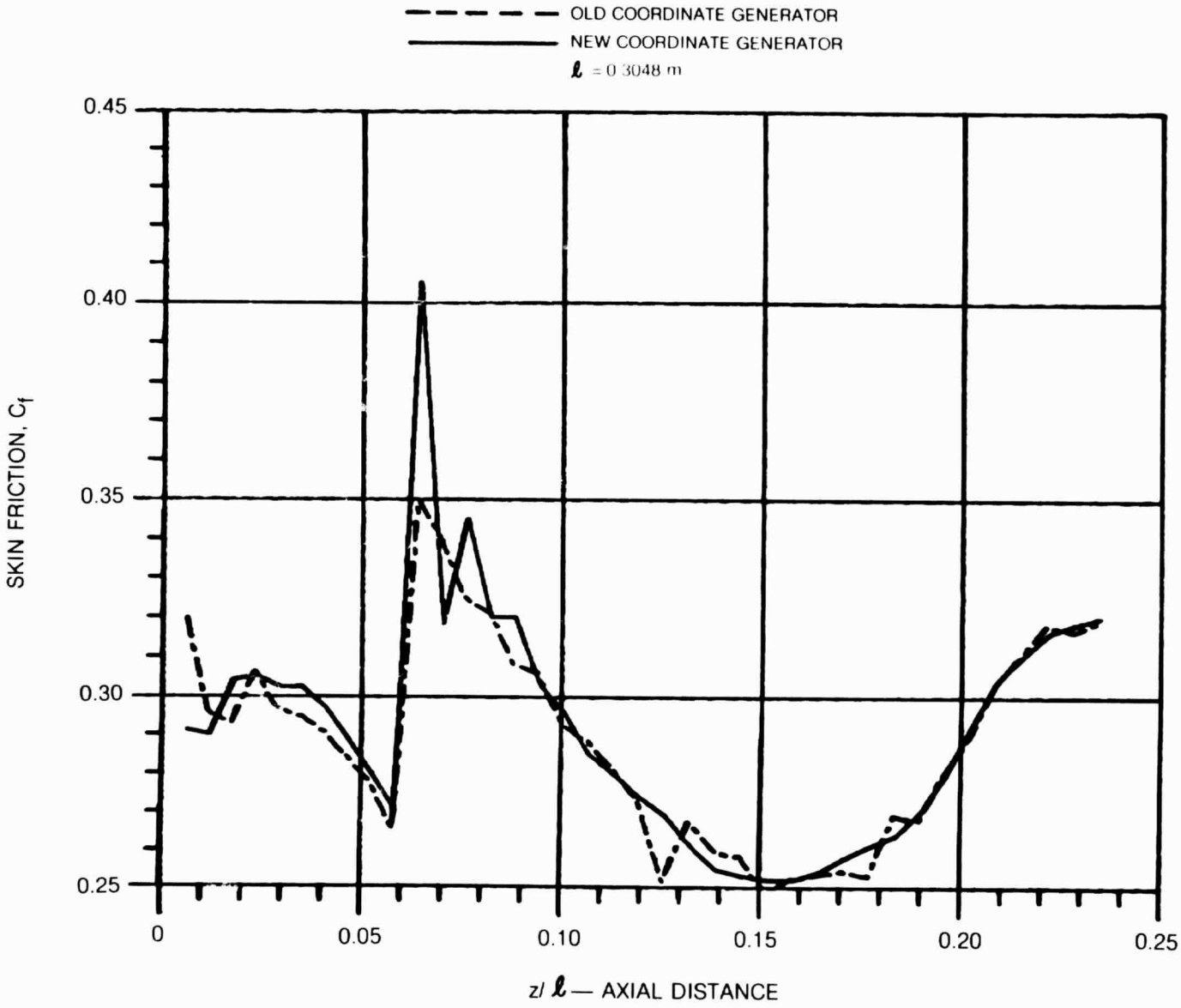

Fig. 17. Comparison of the Inner Wall Skin Friction Calculated with New and Old Grid Generators

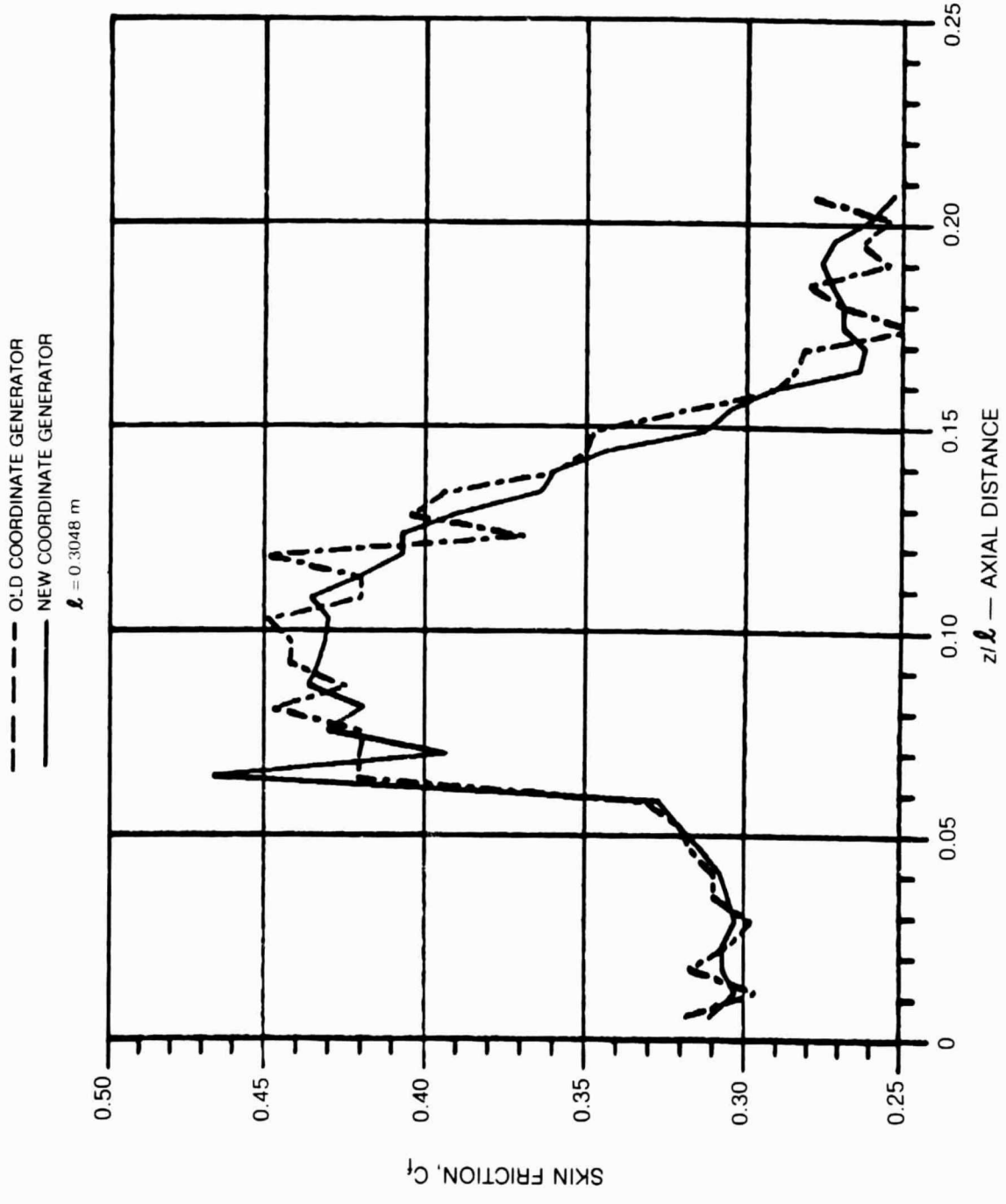

Fig. 18. Comparison of the Outer Wall Skin Friction Calculated with New and Old Grid Generators

81-10-63-14

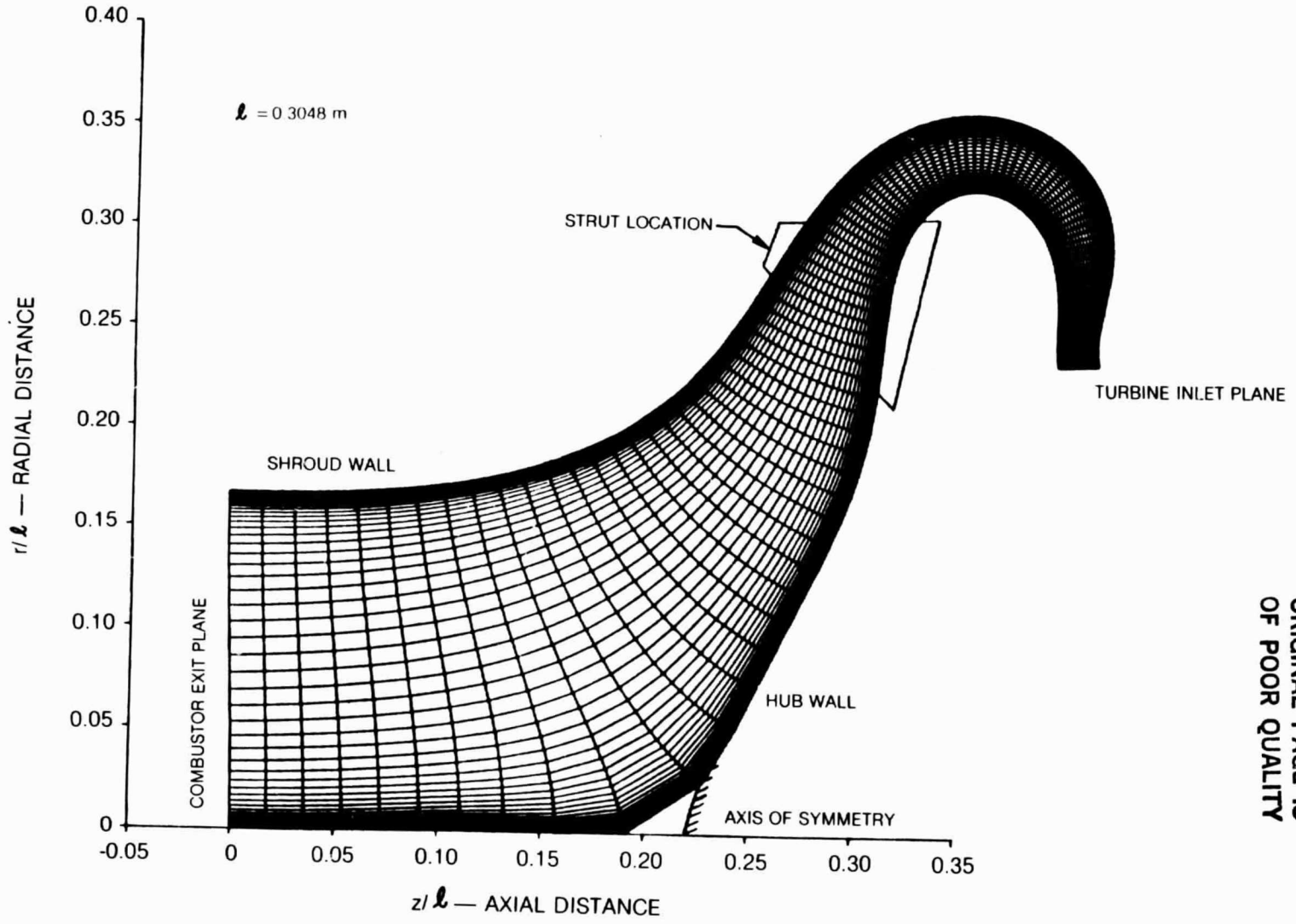

Fig. 19. Computational Mesh for AGT101 Turbine Inlet Duct

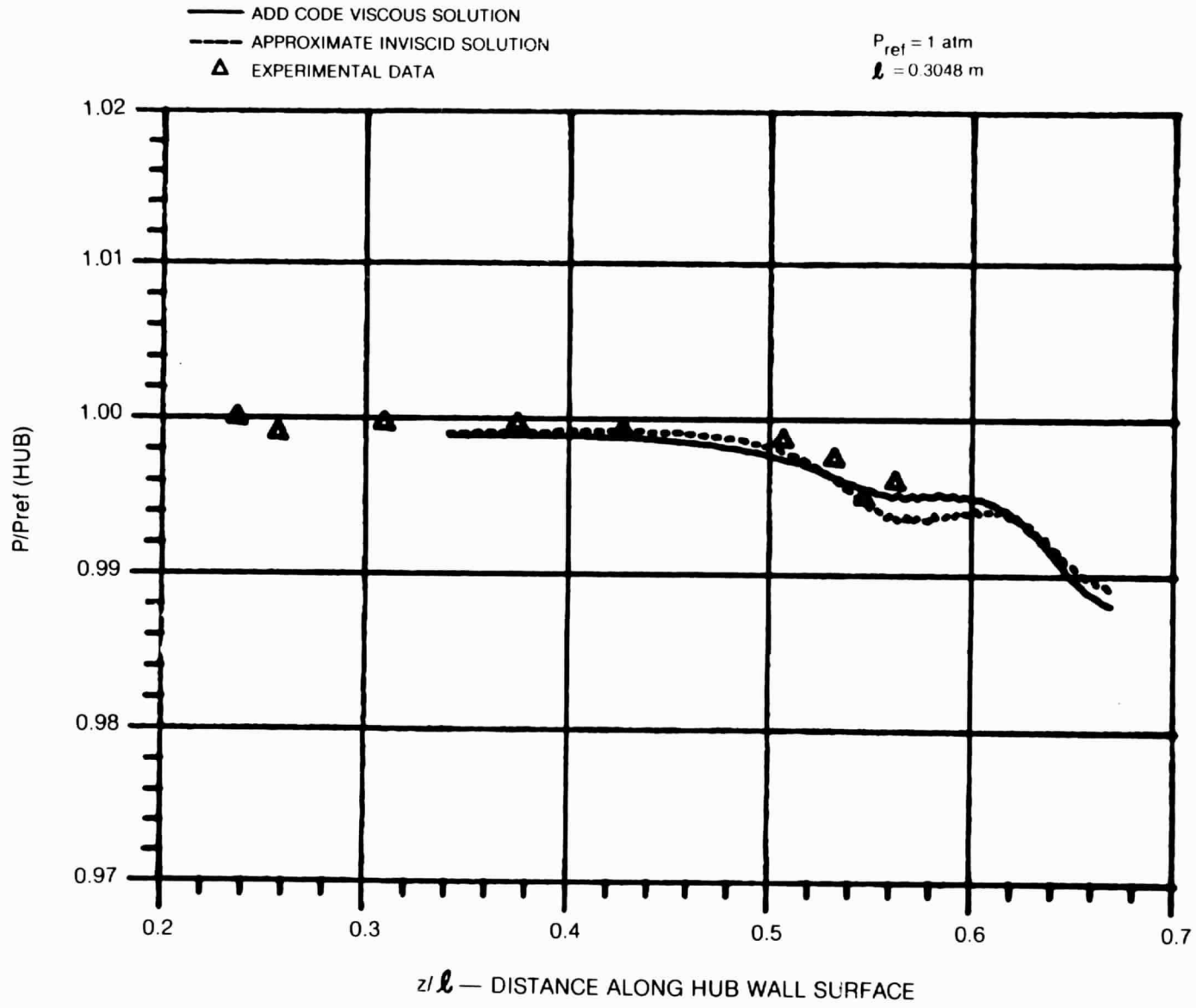

Fig. 20. Hub Wall Static Pressure Distribution for AGT101 Turbine Inlet Duct

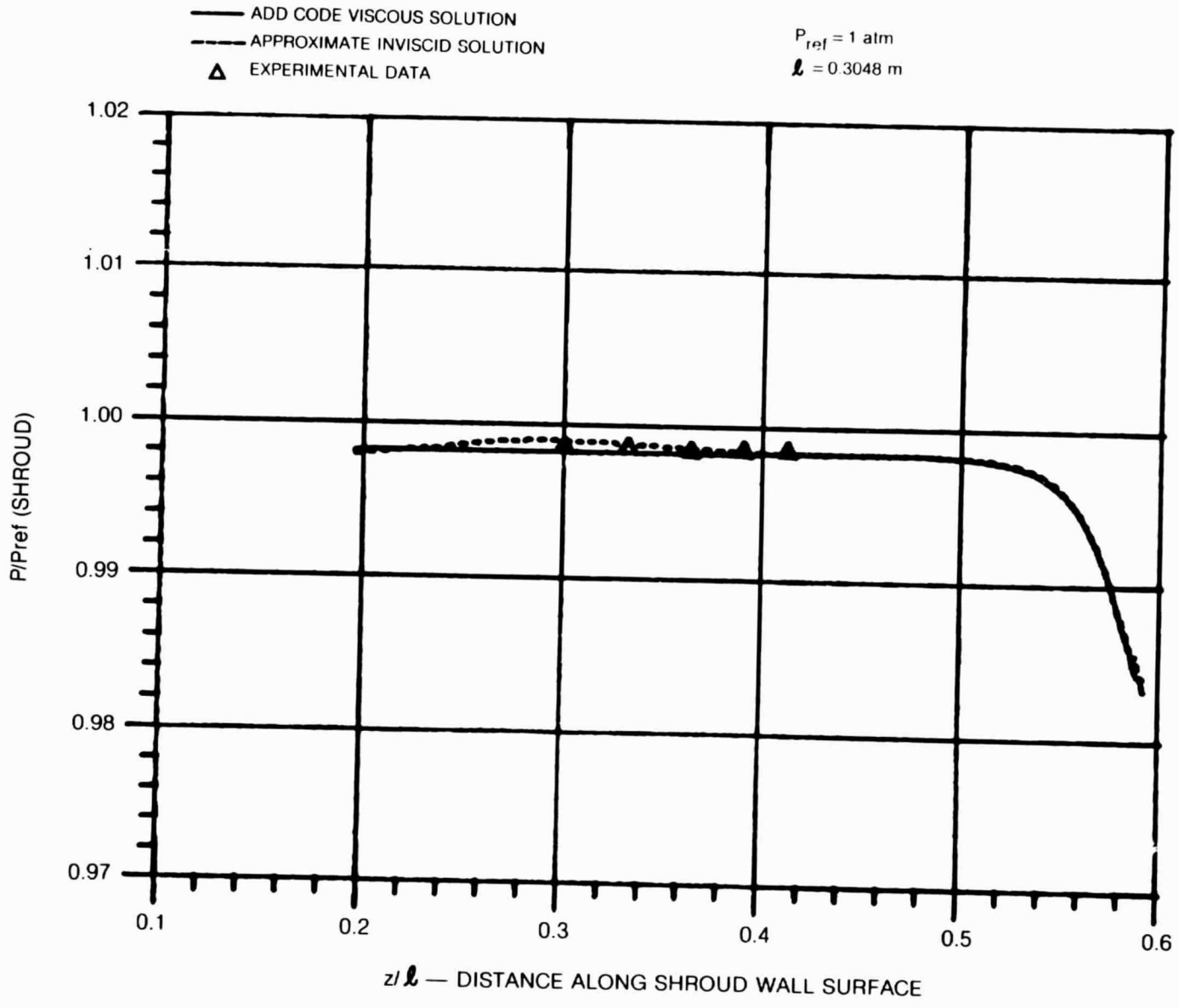

Fig. 21. Shroud Wall Static Pressure Distribution for AGT101 Turbine Inlet Duct

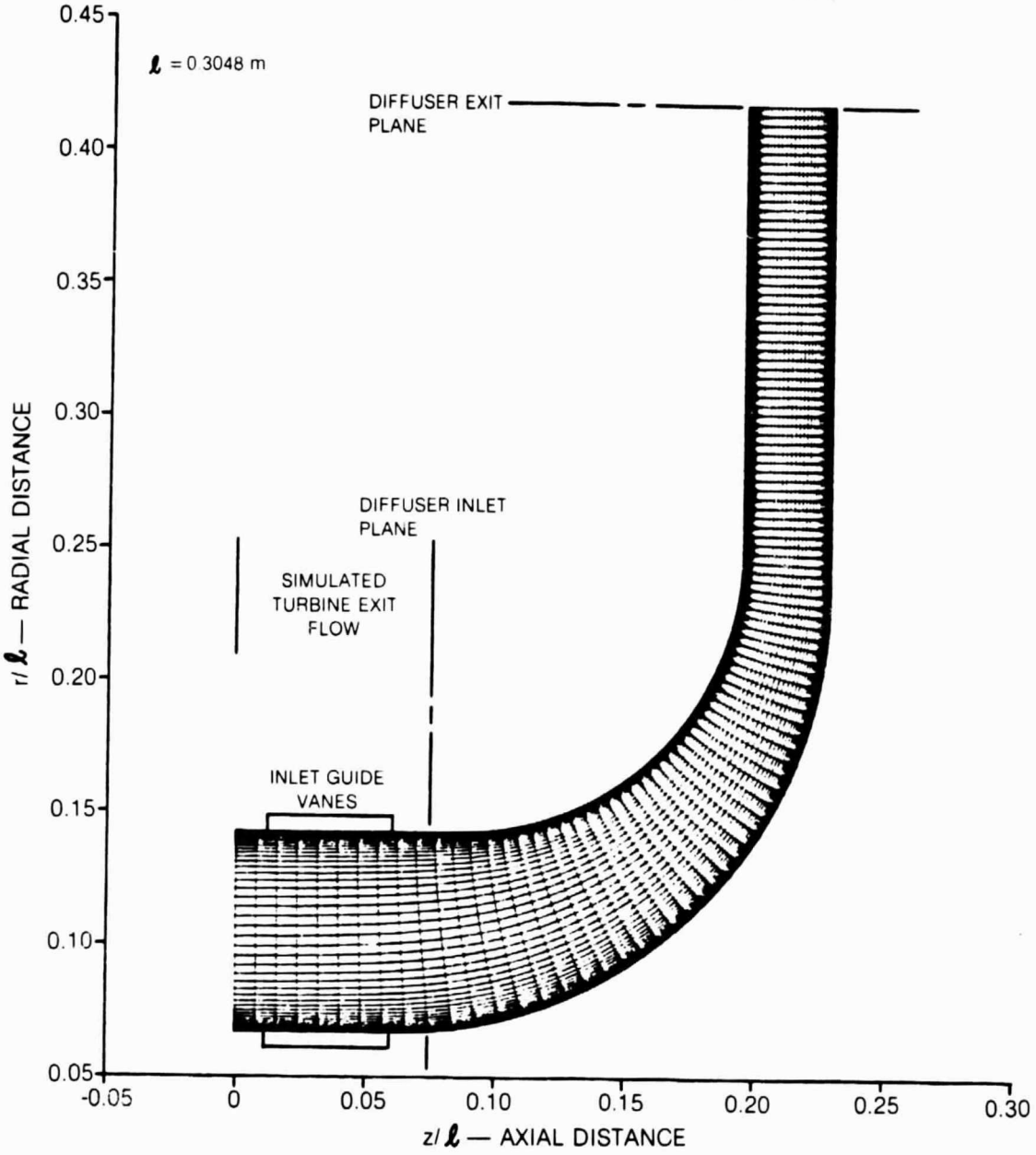

Fig. 22. AGT101 Exhaust Diffuser

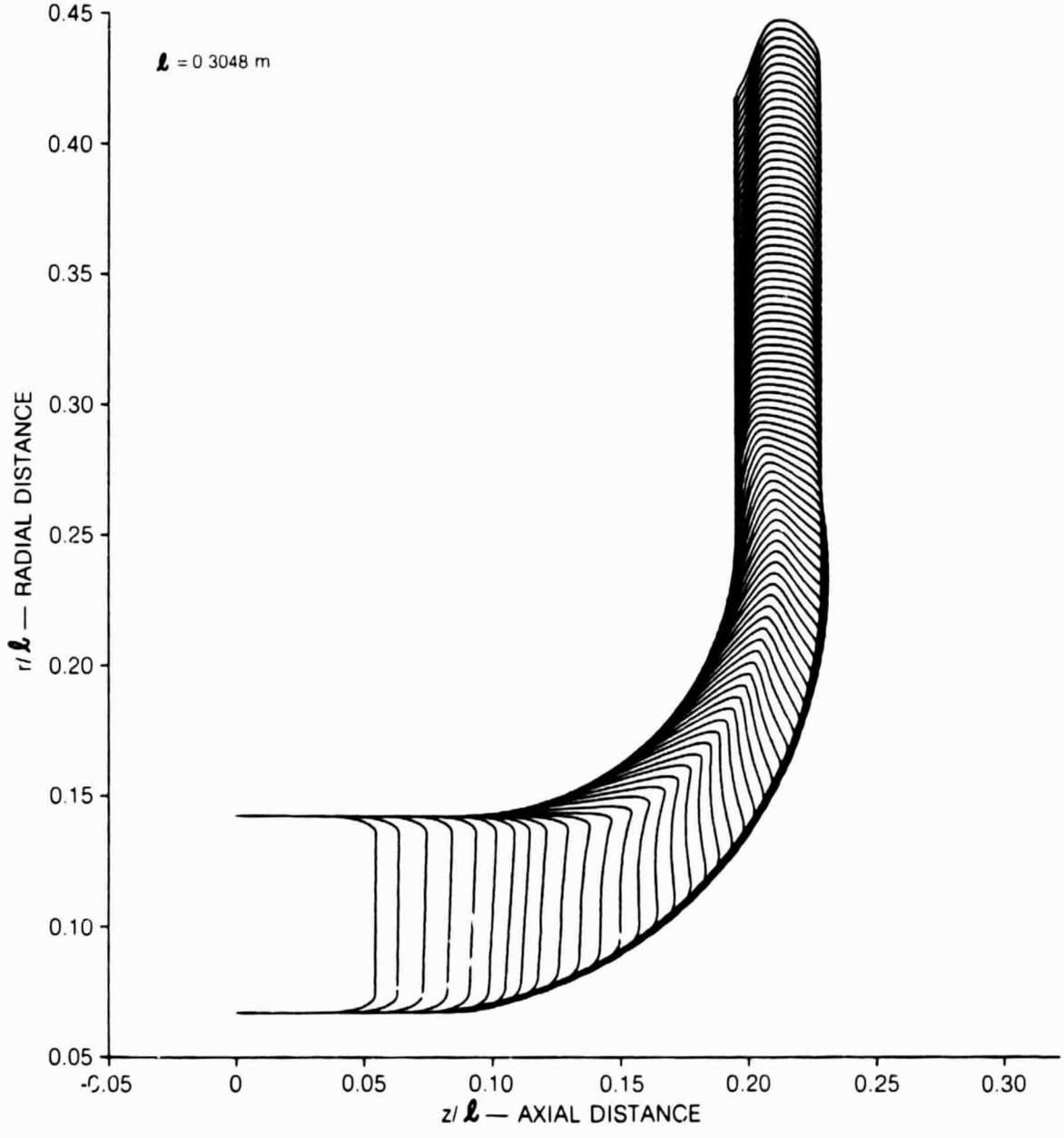

Fig. 23. Streamwise Velocity Distributions in AGT101 Exhaust Diffuser

81-10-63-27

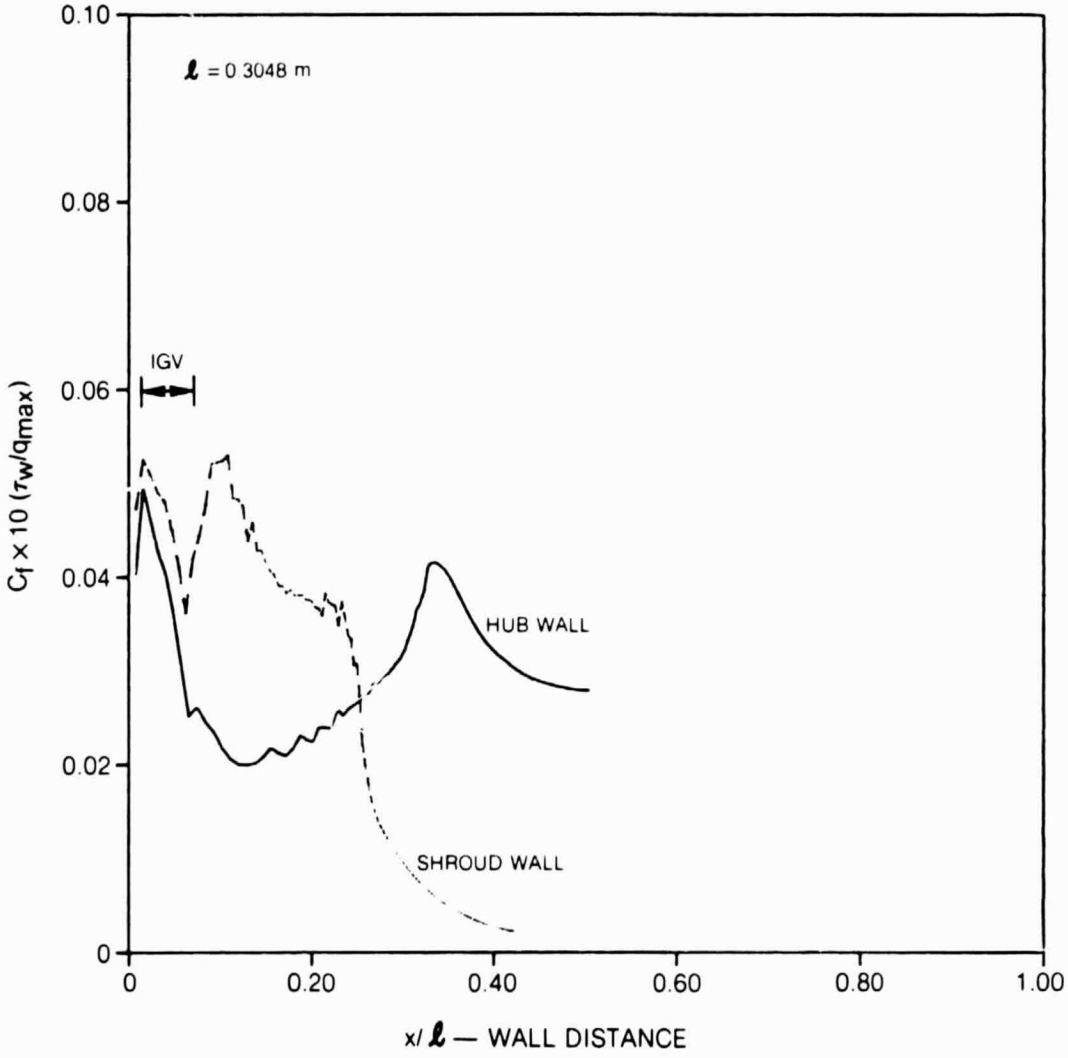

Fig. 24. Calculated Wall Friction Coefficient on Hub and Shroud Walls in AGT101 Exhaust Diffuser

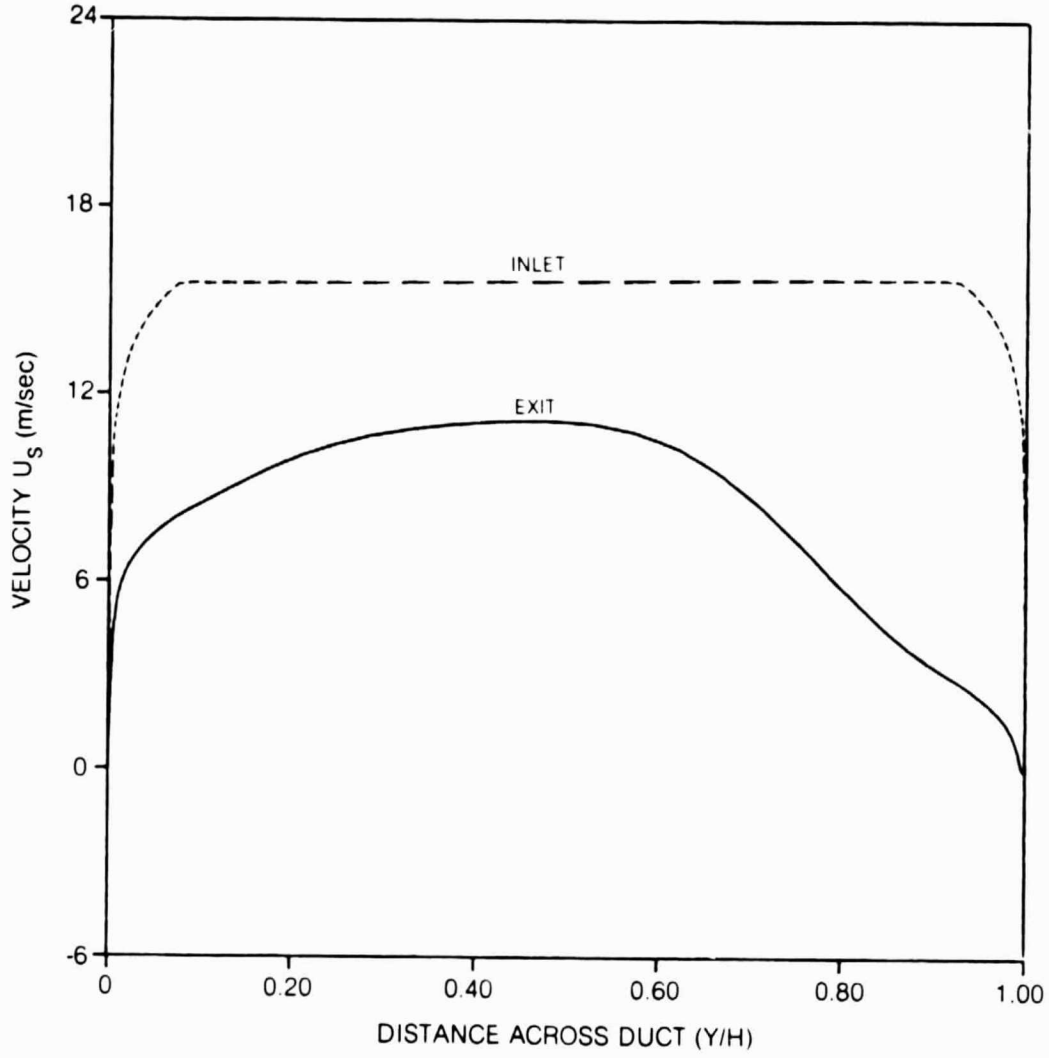

Fig. 25. Inlet and Exit Streamwise Velocity Distributions in AGT101 Exhaust Diffuser

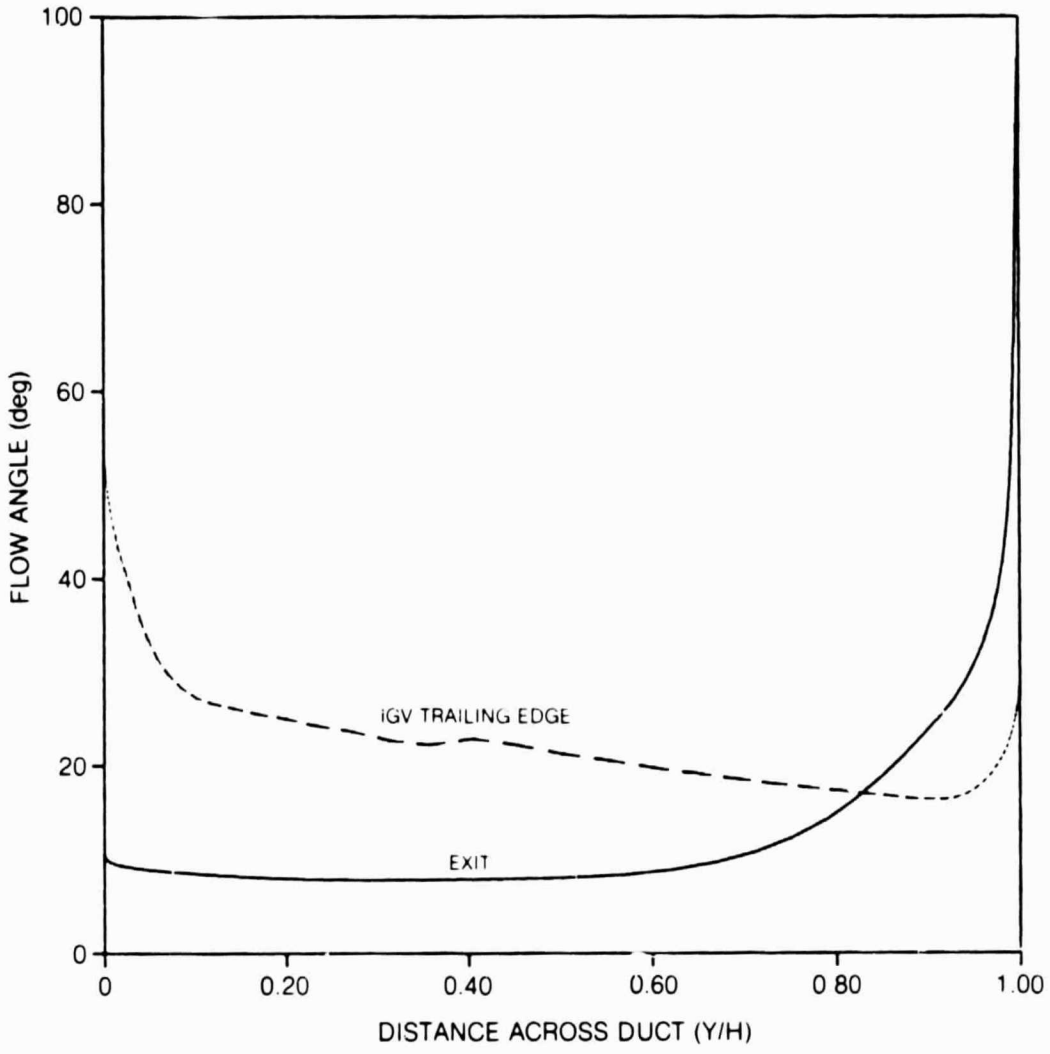

Fig. 26. Flow Angle Distributions IGV Trailing Edge and Exit for AGT101 Exhaust Diffuser

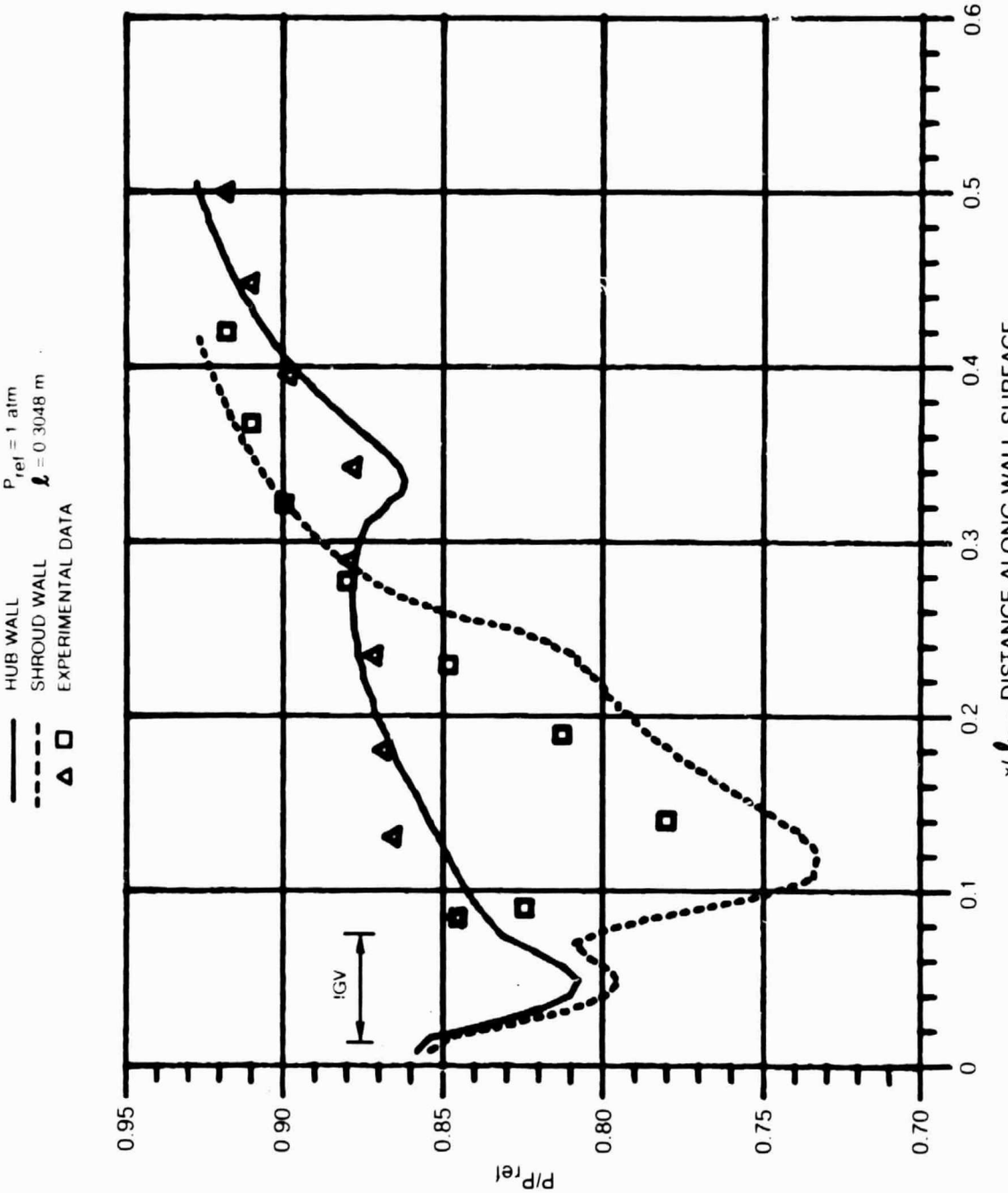

Fig. 27. Calculated and Measured Pressure Distribution in AGT101 Exhaust Diffuser

81-10-63-28